Evaluating the controls of shear stress, sediment supply, alluvial cover, and channel morphology on experimental bedrock incision rate

Joel P. L. Johnson[1] and Kelin X. Whipple[2]

Received 1 April 2009; revised 23 December 2009; accepted 7 January 2010; published 19 June 2010.

[1] We explored the dependence of experimental bedrock erosion rate on shear stress, bed load sediment flux, alluvial bed cover, and evolving channel morphology. We isolated these variables experimentally by systematically varying gravel sediment flux Q_s and water discharge Q_w in a laboratory flume, gradually abrading weak concrete "bedrock." All else held constant, we found that (1) erosion rate was insensitive to flume-averaged shear stress, (2) erosion rate increased linearly with sediment flux, (3) erosion rate decreased linearly with the extent of alluvial bed cover, and (4) the spatial distribution of bed cover was sensitive to local bed topography, but the extent of cover increased with Q_s/Q_t (where Q_t is flume-averaged transport capacity) once critical values of bed roughness and sediment flux were exceeded. Starting from a planar geometry, erosion increased bed roughness due to feedbacks between preferential sediment transport through interconnected topographic lows, focused erosion along these zones of preferential bed load transport, and local shear stresses that depended on the evolving bed morphology. Finally, continued growth of bed roughness was inhibited by imposed variability in discharge and sediment flux, due to changes in spatial patterns of alluvial deposition and impact wear. Erosion was preferentially focused at lower bed elevations when the bed was cover-free, but was focused at higher bed elevations when static alluvial cover filled topographic lows. Natural variations in discharge and sediment flux may thus stabilize and limit the growth of roughness in bedrock channels due to the effects of partial bed cover.

Citation: Johnson, J. P. L., and K. X. Whipple (2010), Evaluating the controls of shear stress, sediment supply, alluvial cover, and channel morphology on experimental bedrock incision rate, *J. Geophys. Res.*, *115*, F02018, doi:10.1029/2009JF001335.

1. Motivation

[2] At the spatial scale of a bedrock river reach, the topography of the channel bed is a first-order control on spatial patterns of both basal shear stress and local sediment flux. Feedbacks between channel incision rate, bed roughness, shear stress and sediment flux are poorly understood yet fundamental to how fast channels will respond to changes in boundary conditions, including hillslope processes and discharge variability at short timescales and climate and tectonics over longer timescales.

[3] A variety of empirical and theoretical models have been proposed to predict bedrock incision rates and patterns along river networks. The intuitive assumption that bedrock incision should increase with increasing fluid shear stress, supported by some field data [*Howard and Kerby*, 1983], forms the basis of the shear stress (or stream power) family of erosion models [e.g., *Howard et al.*, 1994; *Stock and Montgomery*, 1999; *Whipple and Tucker*, 1999, 2002; *Whipple et al.*, 2000]. In this approach the combined effects of multiple erosion processes can be empirically calibrated to coefficients based on field data. However, lumping processes, and their different sensitivities to discharge and sediment flux, limits the predictive ability of these models, particularly when applied to spatial scales as small as channel reaches and timescales as short as flood events. In the saltation-abrasion model [*Sklar and Dietrich*, 1998, 2001, 2004, 2006], sediment flux rather than fluid discharge is the dominant driver of erosion, and incision rates have both positive and negative dependencies on sediment flux: the *tools effect*, in which higher sediment flux increases erosion rate due to more bed impacts, and the *cover effect*, in which higher sediment flux leads to greater local deposition, mantling the bed and shielding it from impact wear.

[4] Recent field studies have found evidence to support tools and cover effects on incision rates, through both short-term monitoring of sediment transport and bedrock incision [*Turowski et al.*, 2007a; *Johnson et al.*, 2010; *Turowski and Rickenmann*, 2008] and by interpreting patterns of bedrock river downcutting over long timescales [*Cowie et al.*, 2008; *Johnson et al.*, 2009]. Sediment flux–dependent models that include positive and negative feedbacks on incision rate are

[1]Jackson School of Geosciences, University of Texas at Austin, Austin, Texas, USA.
[2]School of Earth and Space Exploration, Arizona State University, Tempe, Arizona, USA.

0148-0227/10/2009JF001335

among the models that can simulate fluvial landscape forms including hanging valleys, knickpoints, and slope variability between adjacent channels [e.g., *Gasparini et al.*, 2006; *Wobus et al.*, 2006a, 2006b; *Brocard and van der Beek*, 2006; *Johnson et al.*, 2009]. However, the relationship between landscape form and a particular surface process model is typically nonunique [e.g., *Whipple and Tucker*, 2002], making morphological similarity necessary but not sufficient for validating a particular process model. In addition, process-based incision models often require better temporal and spatial constraints on variables (e.g., discharge, sediment flux, channel morphology) than can feasibly be measured in most field settings over a large parameter space, making model validation difficult.

[5] In this paper, we attempt to evaluate the form of proposed bedrock incision models by using controlled laboratory experiments to explore feedbacks between incision rate, basal shear stress, sediment flux, alluvial cover and evolving bed roughness for the case of river incision by abrasion. These independent and dependent variables are explicitly required, parameterized as a function of the other variables, or implicit in many bedrock erosion models. The flume experiments are idealizations of nature, but allow us to independently control variables that tend to be coupled in nature, letting us explore a range of parameter space.

[6] We use our experiments to evaluate the terms of a generic equation for sediment flux–dependent bedrock channel incision, based on the saltation-abrasion model [*Sklar and Dietrich*, 2004]:

$$E \propto Q_s \cdot Fe \cdot f(\tau)^a, \tag{1}$$

where E is erosion rate, Q_s is sediment flux, Fe is the spatial fraction of bedrock exposed on the channel bed (i.e., not covered by sediment), τ is basal shear stress, and the shear stress term is raised to exponent a. While the right-hand side terms of (1) are not independent in that Q_s and Fe should also depend on τ, this formulation is useful to mechanistically isolate controls on E. Following *Sklar and Dietrich* [2004], we use $f(\tau) = \tau/\tau_{cr} - 1$, where τ_{cr} is the critical shear stress necessary to initiate sediment motion. The quantity $\tau/\tau_{cr} - 1$ is referred to as the excess shear stress, and is zero at $\tau = \tau_{cr}$. Equation (1) is a parsimonious description of bedrock erosion rate that incorporates tools, cover and sediment transport dynamics in a manner consistent with the saltation-abrasion model [*Sklar and Dietrich*, 2004], although (1) neglects a range of dimensional coefficients as well as a possible reduction in erosion rate at high shear stress as sediment becomes suspended.

1.1. Erosional Dependence on Shear Stress

[7] In the theoretical case that all other parameters are held constant, it is unknown whether bedrock incision rates increase, remain unchanged or decrease with increasing fluid basal shear stress. Each of these dependencies has been proposed in recent fluvial bedrock incision models, corresponding to a range of proposed values for exponent a: $a \geq 1$, $a = 0$, $a = -0.5$. In the saltation-abrasion model [*Sklar and Dietrich*, 2004], the exponent on excess shear stress is negative ($a = -0.5$), predicting that erosion rate will decrease with increasing shear stress, all else (e.g., sediment flux, alluvial cover) held equal. This scaling arises from an explicit parameterization of bed load saltation trajectories and their dependence on τ assuming a smooth, planar bed: saltation hop length increases with τ, reducing the number of particle impacts per unit bed area per time on a planar bed and thus counteracting a smaller increase in the vertical (normal to the bed) impact velocity with τ.

[8] *Chatanantavet and Parker* [2009] proposed a variation on equation (1) for bed load erosion in which $a = 0$, i.e., $E \propto Q_s \cdot Fe$. *Parker* [1991] studied downstream fining of clasts due to wear, and found no direct dependence on shear stress. *Chatanantavet and Parker* [2009] reasoned that impact wear on the bed should be proportional to impact wear on bed load clasts, hence $a = 0$.

[9] A range of positive values for shear stress exponent a have also been proposed, both with and without explicit sediment load considerations. *Howard and Kerby* [1983] found that channel incision rate scaled as τ^a with $a \approx 1$ in rapidly eroding badlands. Based on scaling relations between discharge, fluid stresses and sediment transport, *Whipple and Tucker* [1999] and *Whipple et al.* [2000] argued that a should depend on erosion process, and propose $1 \leq a \leq 5/2$ depending on whether plucking, bed load impact wear, or suspended load wear is the dominant erosion mechanism.

1.2. Erosional Dependence on Alluvial Cover

[10] The saltation-abrasion model [*Sklar and Dietrich*, 2004] assumes that the spatial extent of static alluvial patches increases as sediment flux increases, and zero bedrock is exposed where total sediment flux Q_s equals or exceeds total sediment transport capacity Q_t. Averaged over spatial and temporal variations along a channel reach, bedrock exposure Fe is predicted to vary as a linear function of Q_s and Q_t:

$$Fe = 1 - \frac{Q_s}{Q_t}. \tag{2}$$

Flume experiments of *Chatanantavet and Parker* [2008] support the general form of equation (2).

[11] *Sklar and Dietrich* [2004] assume that the presence of sediment in active transport does not inhibit erosion, up to the point where the local bedrock bed is covered by a static alluvial deposit and local erosion rate drops to zero. In contrast, *Turowski et al.* [2007b] hypothesized that erosion may be inhibited not only by static alluvium but also by "dynamic" cover effects, in which sediment is mobile but the local erosion rate is nonetheless reduced (e.g., high concentrations of grains near the bed may reduce impact intensities). On theoretical grounds and consistent with the general form of some experimental results [*Sklar and Dietrich*, 2001], *Turowski et al.* [2007b] proposed that dynamic cover should vary exponentially with Q_s/Q_t, rather than linearly:

$$Fe = e^{\varphi(-Q_s/Q_t)}, \tag{3}$$

where φ should depend in some way on bed topography and is assumed to be 1 in the absence of additional constraints. When combined with a linear tools effect term (i.e., $E \propto Q_s Fe$), the exponential cover model predicts a maximum erosion rate at $Q_s = Q_t$.

[12] One reason *Turowski et al.* [2007b] emphasized dynamic rather than static cover effects is their interpretation that when reach-averaged sediment flux (averaged both spatially and temporally) is less than reach-averaged transport capacity, static alluviation cannot occur anywhere along a channel because a positive feedback would occur where the excess transport capacity would entrain any static sediment. However, flume experiments [*Johnson and Whipple*, 2007; *Chatanantavet and Parker*, 2008] have demonstrated that even when overall $Q_s < Q_t$, local deposition can occur because local sediment flux and transport capacity depend on local bed topography and need not match the averaged or total values in a channel reach (by "local" we mean over a given small subset of bed area, such as a short distance along the bottom of an inner channel).

[13] Based on the flume experiments of *Chatanantavet and Parker* [2008], we hypothesize that the dependence of alluvial cover on Q_s/Q_t follows equation (2) rather than (3). Combining (1) and (2), the generic erosion equation that includes sediment and shear stress sensitivities becomes

$$E \propto Q_s\left(1-\frac{Q_s}{Q_t}\right)\left(\frac{\tau}{\tau_{cr}}-1\right)^a. \quad (4)$$

Equation (4) represents a set of testable hypotheses: (1) erosion rate is linear in Q_s (all else held equal, including *Fe*), (2) *Fe* is linearly related to Q_s/Q_t, (3) erosion rate scales linearly with *Fe*, (4) erosion scales with excess shear stress to power *a* which can be determined from laboratory data, and (5) the combination of these factors can accurately predict reach-averaged experimental erosion rates. If dynamic rather than static cover effects are dominant, then equation (3) should provide a better fit to experimental data than (2). Another prediction of dynamic cover effects is that erosion should be inhibited uniformly and broadly in zones of concentrated sediment transport, not exclusively under patches of static cover. We later interpret the relative importance of static and dynamic cover effects from our experiments.

2. Methods

[14] We conducted our experiments in a laboratory flume 4 m long and 0.3 m wide. The flume frame was twice this wide, but we divided it down the middle in order to conduct two experiments with one batch of uniform strength concrete. To simulate bedrock we used a weak concrete made from well-sorted quartz sand (D_{50} 120 μm) and Portland type 3 (quick setting) cement in a 15:1 ratio by dry weight, fully cured under standing water. Equivalent concrete test batches gave a tensile strength of 0.36 ± 0.24 MPa (2 standard deviations, 6 measurements, Brazil test) for this mix, consistent with *Sklar and Dietrich* [2001]. A small fraction of the cement became clumped and inadvertently was not fully mixed with the sand, resulting in occasional ~1–5 mm embedded hard cement chunks. We interpret that they exerted negligible control on erosion rates and patterns because their size was much smaller than the erosional morphologies that developed. Erosion experiments of *Sklar and Dietrich* [2001], *Chatanantavet and Parker* [2006], *Johnson and Whipple* [2007], and *Finnegan et al.* [2007] used similar weak concrete mixtures to imitate bedrock.

[15] Sediment was distributed uniformly across the upstream flume width at controllable feed rates (Q_s) from 25 to 215 g/s using an auger-type volumetric feeder. Sediment was caught in a downstream settling basin and did not recirculate with the water. We used two well-sorted gravels in different time steps: median intermediate diameter D_{50} = 5.5 mm (D_{10} = 4.2, D_{90} = 6.6), and D_{50} = 2.7 mm (D_{10} = 2.1, D_{90} = 3.2 mm; sizes measured with a Horiba Camsizer). A pump recirculated water at a controllable discharge (Q_w) from 7 to ~80 l/s, providing a range of flume-averaged shear stresses. We measured Q_w using an ultrasonic travel time flowmeter mounted on the flume inlet pipe. Flow depths were measured by hand at five fixed locations along the flume (accuracy ~ ± 5 mm), and were used to calculate water surface slope and flume-averaged flow velocities. Surface velocities were calculated from stopwatch measurements of float travel times. Water jetted off unobstructed from the downstream end of the flume.

[16] We measured the spatial distribution of sediment during active transport through image processing of photographs taken oblique to the bed, looking through flowing water to the flume bed and gravel. Gravel was painted bright red, and the camera flash captured the moving clasts without blurring. Ten to fifteen photographs were taken at each of four locations along the flume. The oblique camera view was corrected for distortion (rectified) assuming a planar bed, and the four images were merged to form a single image covering the bed area. Because of the rough bed topography and water surface distortion, position uncertainties were ± 5 mm (2σ) in x (cross stream) and ± 40 mm (2σ) in y (downstream). Threshold filtering transformed the rectified images into binary, with red pixels classified as sediment (1 if sediment, zero if not). The binary sediment images were then averaged (stacked), and the final result reflects the fraction of the 10–15 photographs in which a grain was identified at a given location. We refer to these measurements as maps of "relative sediment concentration"; they represent the fraction of time that sediment is present at a given location. Relative sediment concentrations could only be measured accurately in time steps with discharges at or lower than ~35 l/s; at higher flow the water became foamy due to increased turbulence in the head box and surfactants released by the paint on the sediment.

[17] The longitudinal slope of the initial bed surface was 0.065. This slope was chosen based on calculations that shear stresses at maximum discharge would nearly reach the threshold of partial suspension for the 2.7 mm sediment. During the same experiments, time steps in which we measured impact wear by fully suspended sand were also conducted, and the steep flume slope and large range of grain sizes allowed us to span a wide range of shear stresses for both bed load and suspended load transport. Here we only report on erosion by bed load. The steep bed slope was a tradeoff in our experimental design because it resulted in strongly supercritical flow conditions (Froude numbers *Fr* between 2.4 and 3.5, with $Fr = U/\sqrt{gh}$, where U is mean velocity, g is gravitational acceleration, and h is mean flow depth; Table 1). While our experiments thus reflect imperfect hydrodynamic scaling to nature because the experimental *Fr* numbers are higher than typically observed for bedrock rivers, field observations of bedrock channels during floods have often found supercritical flow conditions ($Fr > 1$)

[e.g., *Tinkler and Parish*, 1998; *Turowski and Rickenmann*, 2008], and previous bedrock incision experiments have been conducted at high *Fr* (e.g., *Wohl and Ikeda* [1997], up to Fr≈1.6; *Johnson and Whipple* [2007], up to 2.5; *Finnegan et al.* [2007], ≈1.4; *Chatanantavet and Parker* [2008], up to *Fr* = 2.4). Consistent with prior experiments with supercritical flow, downstream flow conditions had negligible influence on upstream flow and there was no discernable influence on local erosion rate by the downstream bed topography or outlet conditions [*Shepherd and Schumm*, 1974; *Wohl and Ikeda*, 1997; *Johnson and Whipple*, 2007; *Finnegan et al.*, 2007; *Chatanantavet and Parker*, 2008].

[18] We conducted two experiments (A and B) using one batch of concrete, which we describe below. In our usage, each experiment is made up of multiple "time steps." During an individual time step, Q_w and Q_s were each held constant for a measured amount of time (typically 15 min), during which the concrete bed eroded a minor amount. Surface topography was mapped between time steps using a triangulating laser displacement sensor (Keyence LK-503) and a computer-controlled axis system. We scanned the surface at 2 mm spacing in the cross-stream direction (x) and 5 mm in the longitudinal direction (y), and then interpolated the topography to have a uniform 2 mm spacing in x and y. All standing water and sediment were cleared out of the flume before scanning, so the scans only measure the bedrock surface topography. The surface of alluvial deposits could not be scanned because they were not sufficiently stable to be preserved when turning off sediment flux and water discharge between time steps. Erosion was measured by differencing topographic surface scans taken before and after each time step. To calculate erosion we first removed points where the local bed gradient was > 4 (primarily the nearly vertical lateral slopes of the inner channel margins) because elevation measurements were less accurate on steep slopes. We also removed points in the erosion (difference) maps more negative than −100 μm (i.e., physically unrealistic negative erosion) which were rare and always bad measurements. Individual measurement uncertainty in the erosion maps is ~100 μm (2σ), based on histograms of pixels that give negative erosion and so unambiguously reflect measurement error. The error in *average* erosion rates is less than the 100 μm uncertainty at individual locations.

2.1. Experiment A: Bed Evolution Under Variable Q_w, Q_s

[19] Almost all of the results we present are from experiment A, in which sediment supply and discharge were systematically varied. Table 1 gives the conditions used in each time step. Our overall experimental design was as follows: to isolate the effect of discharge on erosion, we performed three series of time steps with an order-of-magnitude variation in Q_w but constant Q_s (time steps 7–12, 13–18, 30–34). Time steps 7–12 used sediment with a median diameter of 2.7 mm, and the remainder of time steps used 5.5 mm sediment. To isolate the effect of sediment flux on erosion, we varied Q_s under two sets of constant Q_w (time steps 19–24, 25–29). An important limitation of our method was that bed topography evolved due to nonuniform erosion, so even in time steps with constant Q_w or Q_s, the "initial condition" of bed topography for each sequential time step was not constant. We minimized the change in bed topography by running time steps for the shortest time over which we felt erosion could be reliably measured (15 min). While erosion changed bed topography substantially during the course of the entire experiment, topographic changes were relatively minor over the 5–6 time steps that comprise each forcing series. Two advantages of our method in which the bed evolves are that (1) we can explore bed topography and roughness as controls on erosion and (2) the topography naturally developed due to the flow, sediment and lithologic conditions of the particular experiments, rather than imposing an arbitrary bed topography that may superficially look similar to some bedrock channels but that may actually be inconsistent with erosion driven by local conditions.

2.2. Experiment B: Bed Evolution Under Constant Q_w, Q_s

[20] In experiment B, we held Q_w and Q_s constant and allowed topography to evolve, to measure the development of bed roughness under conditions of constant forcing, in contrast to the variable forcing of experiment A. We only present a small number of results from this experiment (in section 3.4 and Figure 10b), to contrast the evolution of bed roughness between the two experiments. In these time steps, discharge was 35 l/s, sediment flux 100 g/s, and sediment size was 5 mm.

3. Results

[21] During experiment A, the coupling of sediment transport and erosion resulted in the gradual incision of a narrow inner channel (Figure 1), due to a positive feedback where sediment became preferentially transported in topographic lows as a result of lateral slope-dependent sediment transport. This topographic focusing of local sediment flux in turn focused erosion in the local lows, because erosion by abrasion can only occur where sediment impacts the bed. Later time steps show the progression of inner channel formation as a result of these feedbacks. The initial condition for bed load erosion was the topography of time step 6, which was lower by 20–30 mm in the middle of the flume compared to the sidewall margins, but nonetheless broadly planar with some roughness due to suspended sand erosion in time steps 1–5 (not shown). Equivalent inner channels developed in experiments of *Johnson and Whipple* [2007] and also *Finnegan et al.* [2007], suggesting that the final erosional morphology was not the result of the initial bed topography, although the zone of initial local lows influenced the particular location of inner channel development. Note the mapped longitudinal centerlines of the inner channel in later time steps, which we use in interpreting local erosion and deposition patterns (Figure 1). The inner channel centerlines were calculated in each time step based on the bed topography, by following the zone of minimum elevation (averaged over a 10 mm width) in each time step. The developing inner channel migrated slightly between sequential time steps due to lateral erosion. Note also in Figure 1 that while elevations appear to increase by several cm downstream, these elevations were measured relative to the planar base of the flume (i.e., the plastic bottom below the poured concrete bed), not relative to horizontal. The flume bottom had a slope of 0.07 but the concrete bed

Table 1. Summary of Experiment A Time Steps and Associated Data[a]

Time Step	Q_s (g/s)	Gravel D_{50} (mm)	Q_w (l/s)	Flow Depth H (mm)	Fr	$\tau/\tau_{cr} - 1$	Q_s/Q_t	Inner Channel Fe	Erosion		Bed Roughness	
									Flume Averaged (mm)	Inner Channel (mm)	Flume Averaged (mm)	Inner Channel (mm)
7	100	2.7	77 ± 5	100	2.9	31	0.04	1	0.24	0.91	9.5	5.2
8	100	2.7	7.5 ± 0.5	20	3.5	7	0.40	1	0.23	0.96	9.6	5.1
9	100	2.7	37 ± 2	60	2.9	24	0.07	1	0.27	1.12	9.8	5.0
10	100	2.7	17.7 ± 0.5	40	2.8	14	0.14	1	0.26	1.01	10.1	4.9
11	100	2.7	56 ± 2	85	2.8	28	0.05	1	0.27	1.22	10.3	5.0
12	100	2.7	80 ± 2	115	2.5	35	0.04	1	0.27	1.51	10.5	5.4
13	100	5.5	82 ± 2	120	2.4	18	0.04	1	0.30	1.30	10.8	5.9
14	100	5.5	8 ± 0.6	20	3.0	3	0.41	1	0.34	2.22	11.3	6.5
15	100	5.5	56 ± 1.5	85	2.8	13	0.05	1	0.33	1.50	11.7	7.1
16	100	5.5	34.8 ± 0.5	60	3.0	10	0.09	1	0.33	1.98	12.1	7.9
17	100	5.5	18 ± 0.5	35	3.1	6	0.18	1	0.34	1.93	12.6	8.6
18	100	5.5	80 ± 1	NA[b]	NA[b]	17[b]	0.04[b]	1	0.33	2.09	13.1	9.4
19	215	5.5	7 ± 1	20	2.7	3	1.08	0.59	0.58	1.56	13.6	8.8
20	25	5.5	7 ± 1	20	2.7	3	0.13	1	0.14	0.86	13.8	9.1
21	150	5.5	7 ± 1	20	2.9	3	0.84	0.70	0.42	1.81	14.3	8.5
22	50	5.5	7.9 ± 0.6	20	3.4	3	0.29	1	0.24	1.74	14.6	8.8
23	100	5.5	6 ± 1	20	2.5	3	0.57	0.82	0.35	2.06	15.1	8.5
24	215	5.5	6.5 ± 1	20	2.7	3	1.17	0.38	0.47	0.43	15.4	8.2
25	215	5.5	34.5 ± 1	60	2.9	9	0.21	0.73	0.53	2.21	16.1	7.7
26	150	5.5	32 ± 0.5	60	2.8	8	0.15	0.93	0.47	2.41	16.8	7.5
27	100	5.5	35.5 ± 0.5	60	3.0	9	0.10	1	0.38	2.54	17.4	7.8
28	50	5.5	34.2 ± 1	60	2.8	9	0.05	1	0.20	1.31	17.7	8.0
29	25	5.5	34.5 ± 1	60	2.8	9	0.02	1	0.11	0.58	17.8	8.1
30	100	5.5	7.1 ± 0.5	20	2.6	3	0.53	0.49	0.25	0.95	18.2	7.7
31	100	5.5	78 ± 3	110	2.6	15	0.04	1	0.40	2.64	18.8	8.2
32	100	5.5	18.7 ± 0.8	40	3.0	6	0.19	0.89	0.31	1.93	19.4	7.9
33	100	5.5	54 ± 1.5	80	2.8	12	0.06	0.90	0.35	2.11	20.0	7.6
34	100	5.5	35.5 ± 1	65	2.6	9	0.10	0.93	0.34	2.06	20.6	7.7

[a]Time steps are organized into series based on either constant Q_s and variable Q_w (7–12, 13–18, 30–34) or constant Q_w and variable Q_s (19–24, 25–29). Each time step lasted 15 min. The amounts of erosion listed represent the average vertical distance of downcutting over each 15 min time step. The flume width was 30 cm and the initial bed slope was 0.065.

[b]Values were either not measured or were estimated.

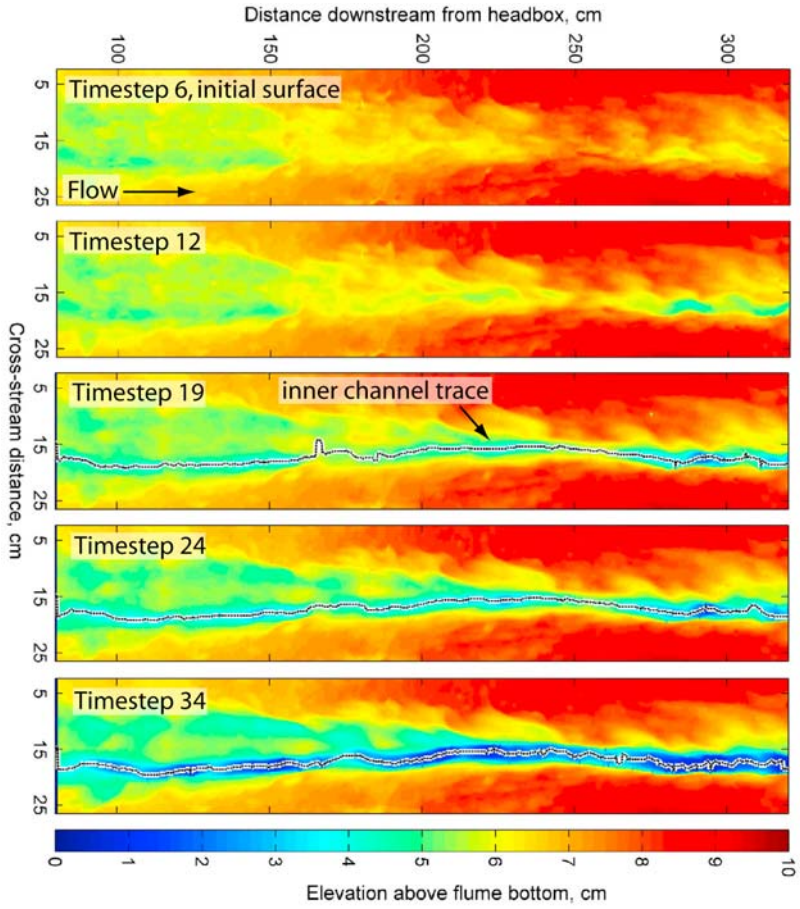

Figure 1. Bed topography in experiment A. The flume is 30 cm wide (starting at zero, *x* axis) and 4 m long (starting at 0, *y* axis). The area shown is the central subset of the flume we use for analysis (80–320 cm downstream from head box, 2.4–26.4 cm from the flume sidewall) to minimize possible inlet, outlet, and sidewall effects. Flow direction is indicated. Initially, the planar bed center was intentionally slightly lower than the sloping bed sides at the flume walls to inhibit sediment transport and incision at the sidewalls. Inner channel centerlines are indicated and described in the text.

thickened slightly downstream, giving an initial bed slope of 0.065.

[22] The spatial distribution of sediment in active transport during each time step is controlled primarily by bed topography, such that bed load becomes focused in the interconnected topographic lows (Figure 2; compare to Figure 1). Relative sediment concentrations represent the fraction of time sediment was present at a given location; values close to 1 indicate the constant presence of sediment. These measurements cannot directly differentiate between stable deposits and grains in active transport. Both local sediment concentrations and the width of the zone of sediment transport increases with Q_s. In the upstream half of the flume, a secondary preferred path for sediment transport is apparent (Figure 2), consistent with lows in the bed topography (Figure 1). Downstream of ~200 cm from the head box, sediment transport is focused along a single inner channel thread. In section 3.2 we make the assumption that the local sediment flux over a given bed area scales with the relative sediment concentration.

[23] Erosion rate and the width of the eroding zone increased with total sediment flux. Figure 3 shows the amount of vertical erosion of the concrete bed (bedrock) that took place during each 15 min time step, for time steps 19–24 with constant discharge (~7 l/s) and variable sediment flux. At low sediment fluxes all of the sediment and erosion are focused at the bottom of the inner channel, while at high sediment fluxes, the zone of erosion widens beyond the margins of the inner channel.

[24] As Q_s increased, erosion at the inner channel bottom first increased, then decreased, and then ceased. At the same time, as Q_s increased the zone of sediment transport widens as the inner channel bottom becomes filled, and higher elevations adjacent to the inner channel are preferentially eroded. Figure 4 illustrates this interplay between topography, erosion and sediment concentration for a channel cross section, averaged over a short longitudinal distance (226–236 cm downstream from head box). The time steps shown (19–24) are a series in which discharge was held constant while sediment flux was varied by nearly an order of magnitude. Note that while the inner channel deepened over the course of these sequential time steps, the overall change in bed topography was relatively minor between time steps 19 and 24 (see Figure 1). *Finnegan et al.* [2007] measured

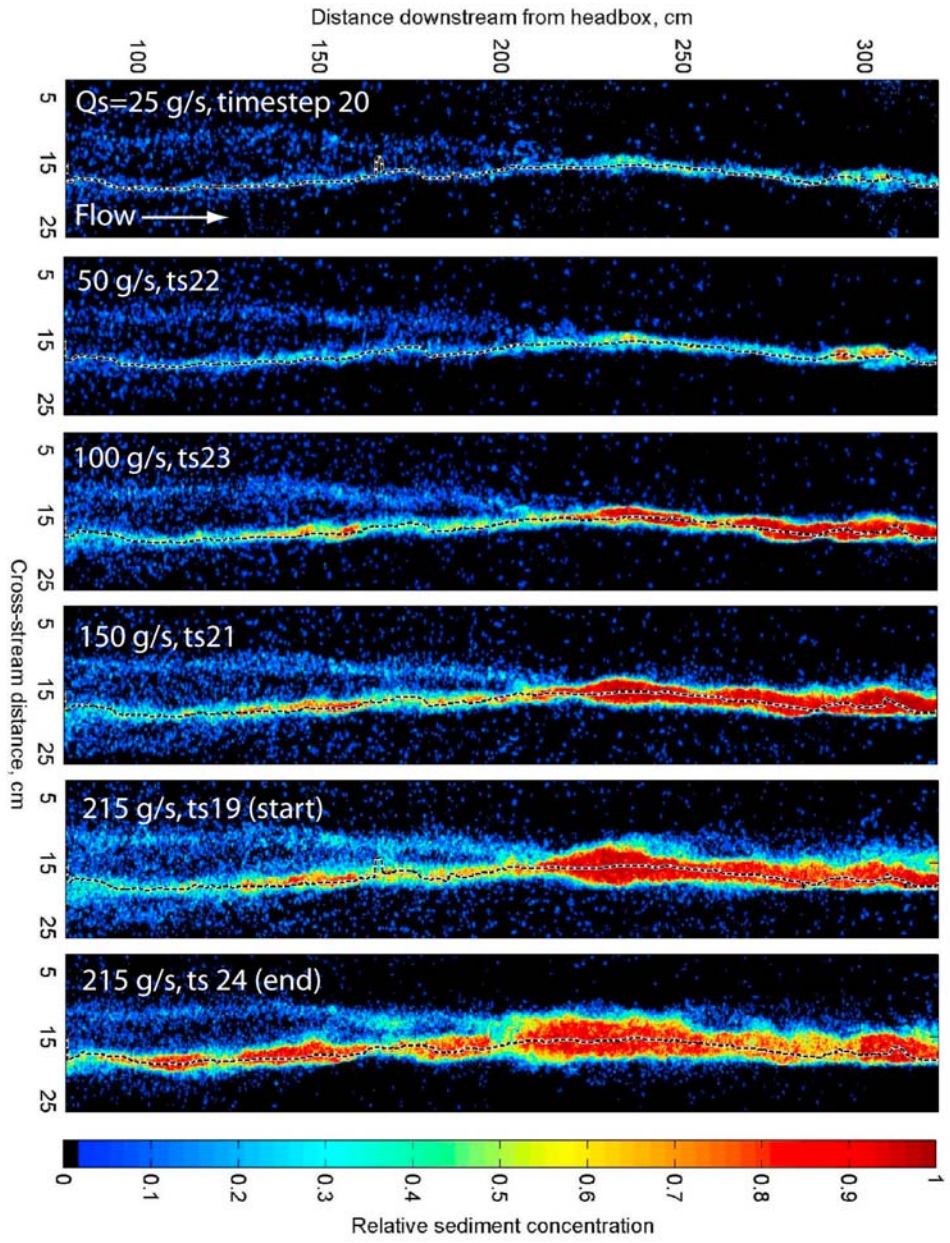

Figure 2. Relative sediment concentration on the flume bed during active transport for a series of time steps (19–24) with variable sediment flux, discharge ~ 7 l/s, and gravel. Inner channel centerlines are indicated. Time steps are shown in order of increasing sediment flux rather than chronologically.

similar patterns of incision and bed topography with increasing sediment flux.

3.1. Sediment Cover

[25] Because static alluvial deposits were not stable enough to be measured directly and the relative sediment concentration maps (Figure 2) cannot differentiate between moving and static sediment, we interpreted cover effects based on erosion maps. We interpret that the decrease of local erosion to zero at the bottom of the inner channel (Figures 3 and 4) at high sediment supply is due to mantling by local alluvial cover. Cover models agree that erosion should cease where a static deposit develops, and we know of no other mechanism to locally and abruptly reduce erosion rate to zero along the axis of the inner channel as Q_s increases (Figure 3). Reaches were only designated as "covered" if they both had minimal erosion in the given time step and were locations of higher erosion in time steps with lower sediment flux. For example, time step 23 (Figure 3, Q_s = 100 g/s), has two patches of zero erosion along inner channel which we interpret as indicating alluvial deposition. The abrupt transitions between earlier high erosion and zero current erosion suggest that stable deposits formed on the bed and completely inhibited local incision. In contrast, the shorter inner channel reaches with no erosion that approximately persist between lower Q_s time steps are downstream-sloping faces that are topographically shadowed from impact

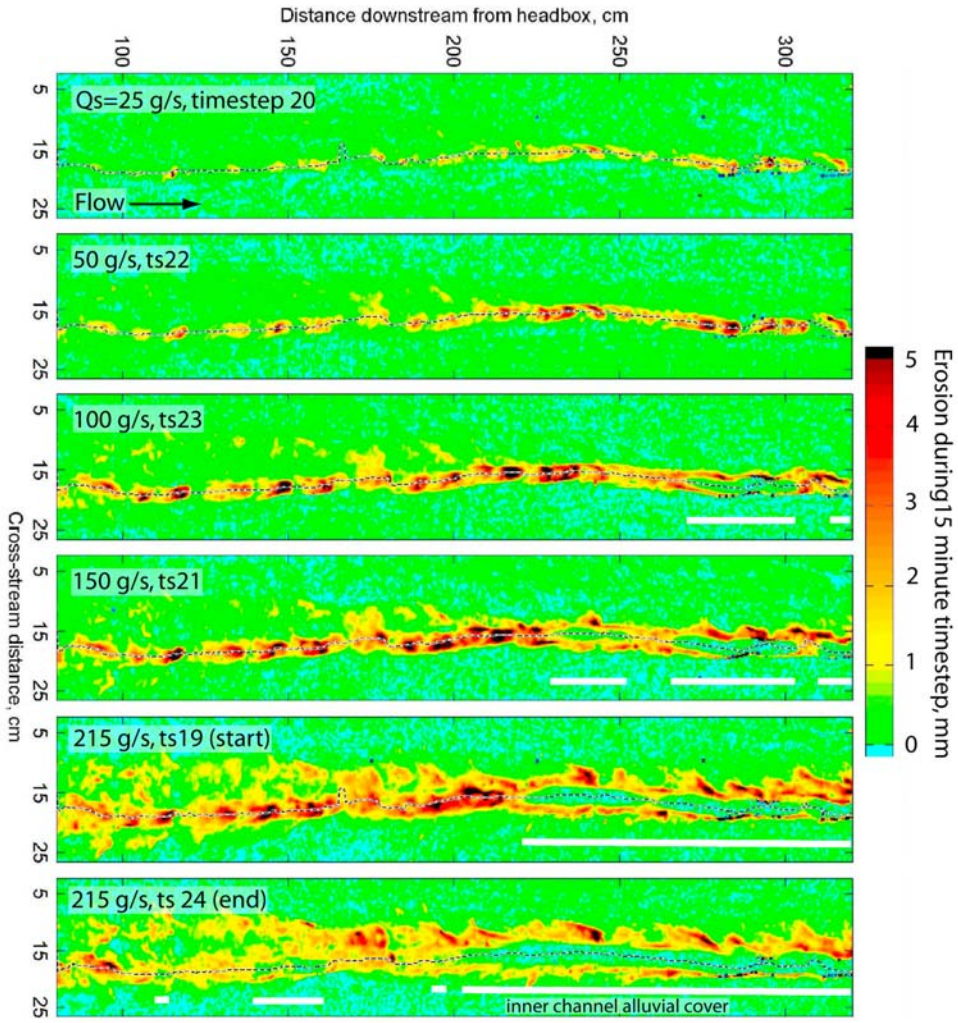

Figure 3. Maps of the amount of vertical erosion that occurred during each 15 min time step for time steps 19 to 24. Water discharge is ~7 l/s, and D_{50} = 5.5 mm. The color map showing erosion has a color break between green and cyan at 0; negative erosion values represent noise. Erosion was locally greater in some places than the color range covers (i.e., >5 mm). Zones of inferred inner channel alluvial cover in each time step are indicated by white lines below the inner channel. Inner channel centerlines are indicated.

wear, and therefore not indicative of cover effects (discussed in section 3.4).

[26] The fraction of bed area exposed, *Fe*, is 1-*Fc*, where *Fc* is fraction of bed area covered. Figure 5 shows *Fc* calculated in three different ways. First, Fc_{tot}, the fraction of total bed area covered, was calculated as A_c/A_{tot}, where A_c is the area of the bed covered in a given time step (measured from erosion maps, with the boundary between uncovered and covered regions determined visually), and A_{tot} is the total flume bottom area shown in Figure 3. Second, we calculate Fc_{act}, the fraction of "active" bed area covered, as A_c/A_{act}, where A_{act} is the area of the bed over which sediment transport occurs for a given set of Q_w and Q_s conditions imposed during a time step. We make a distinction between the total bed area and the active bed area because the total bed area was imposed on the system, while the active bed area reflects a local balance between transport conditions (Q_w and Q_s) and the naturally evolving bed topography. This approach has the benefit of constraining cover effects that developed along local bed topography that was not arbitrarily imposed (e.g., the fixed flume width). In practice, A_{act} was measured by determining the area of bed covered by sediment in the relative sediment concentrations maps (i.e., concentration > 0) (Figure 2). Third, we calculate Fc_{ic} (the fraction of bedrock covered along the inner channel) as L_c/L_{tot}, where L_c is the length of alluvial cover along the centerline of the inner channel (Figures 1 and 3) and L_{tot} is the total length along the centerline of the inner channel. For the inner channel, reporting a linear cover fraction (rather than an areal cover fraction) avoids the uncertainty associated with defining an exact inner channel width based on variably sloping sidewalls.

[27] The overall trend of increasing cover with Q_s is consistent for all of the methods for measuring F_c, although the actual values of the cover fraction vary (Figure 5). Cover initiates at higher Q_s for the higher discharge series (Q_w =

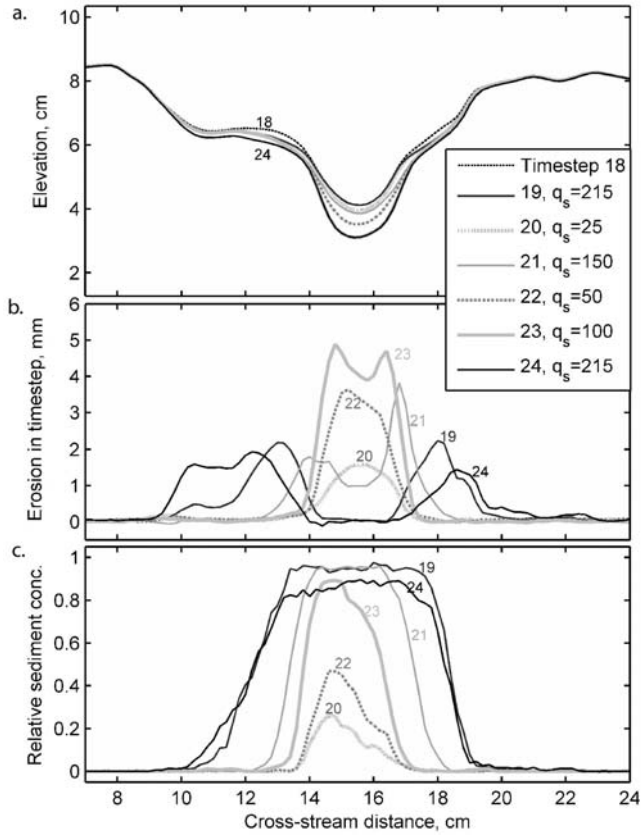

Figure 4. Variations in magnitude and location of erosion with changes in sediment flux averaged over a 10 cm long straight section of inner channel from 226 to 236 cm downstream. (a) Cross-section topography in sequential time steps. Lines from later time steps obscure earlier time steps. (b) Erosion in each cross section per time step. At low Q_s, erosion is focused in the inner channel. With increasing Q_s, inner channel erosion increases but then stops due to deposition, and erosion is focused higher up on the sides and above the inner channel. (c) Relative sediment concentration in each time step, showing how concentration saturates and spreads over a wider area.

35 l/s; time steps 25–29), but static cover increases for both discharge series, once a threshold sediment flux is reached. Importantly, the difference in cover between time steps 19 and 24 illustrates the influence of bed topography on sediment cover (two plotted circles at Q_s = 215 g/s, Q_w = 7 l/s): the time steps had the same forcing but a more deeply incised bed topography in time step 24 due to the cumulative erosion from time steps 20–23 (Figure 5a). In the discussion section we address the causes for the strong spatial variability in cover locations and the nonunique relationship between Q_w, Q_s and cover, due to changes in evolving bed topography.

3.2. Erosion Dependence on Sediment Flux

[28] Next, we evaluate how consistent our data are with model predictions that erosion rate should scale linearly with sediment flux, all else held equal (equations (1) and (4)). Figure 6a shows flume-averaged erosion (the average vertical lowering of the bed area during 15 min time steps) as a function of sediment flux for the two time step series with variable Q_s and constant Q_w. A modest curvature is apparent, with erosion increasing more rapidly at low Q_s than at high Q_s. In contrast, Figure 6b shows erosion over a fixed 10 mm width following the centerline (bottom) of the inner channel for the same time steps. Along the inner channel axis, erosion initially increases with increasing Q_s (tools effect), but then decreases with Q_s once sediment cover is present, demonstrating a cover effect (Figure 5).

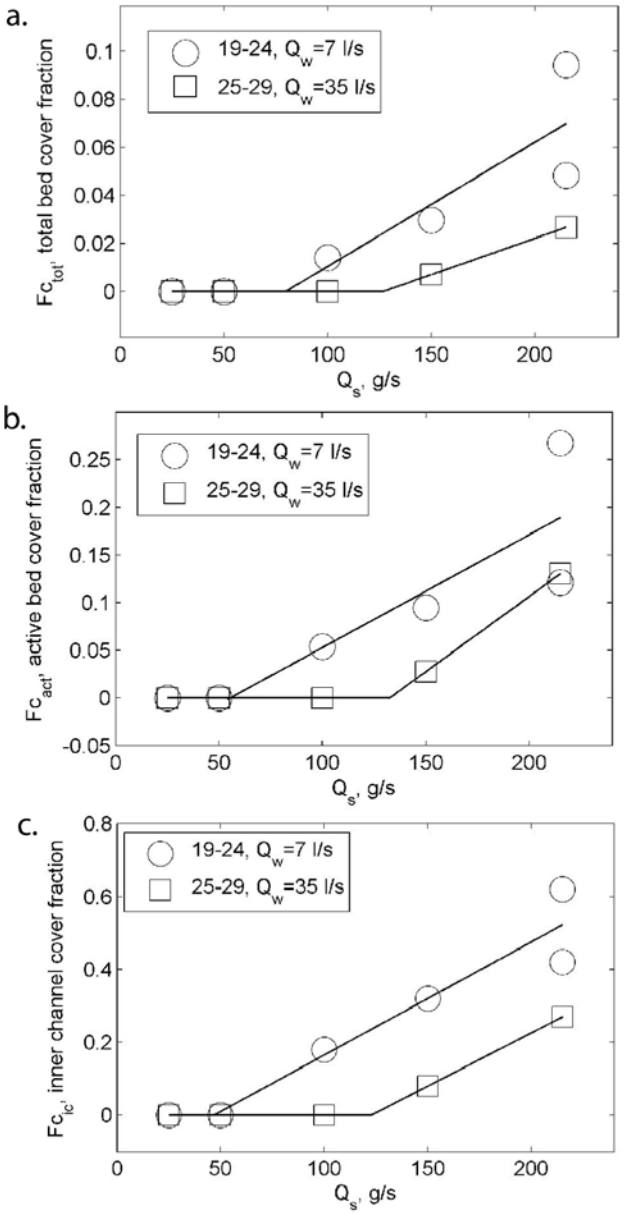

Figure 5. The fraction of the bed covered by alluvium plotted as a function of sediment flux for the two time step series with variable Q_s and constant Q_w. Variables Fc_{tot}, Fc_{act}, and Fc_{ic} represent the cover fractions of the total bed area, active bed area, and inner channel length and are described in the text.

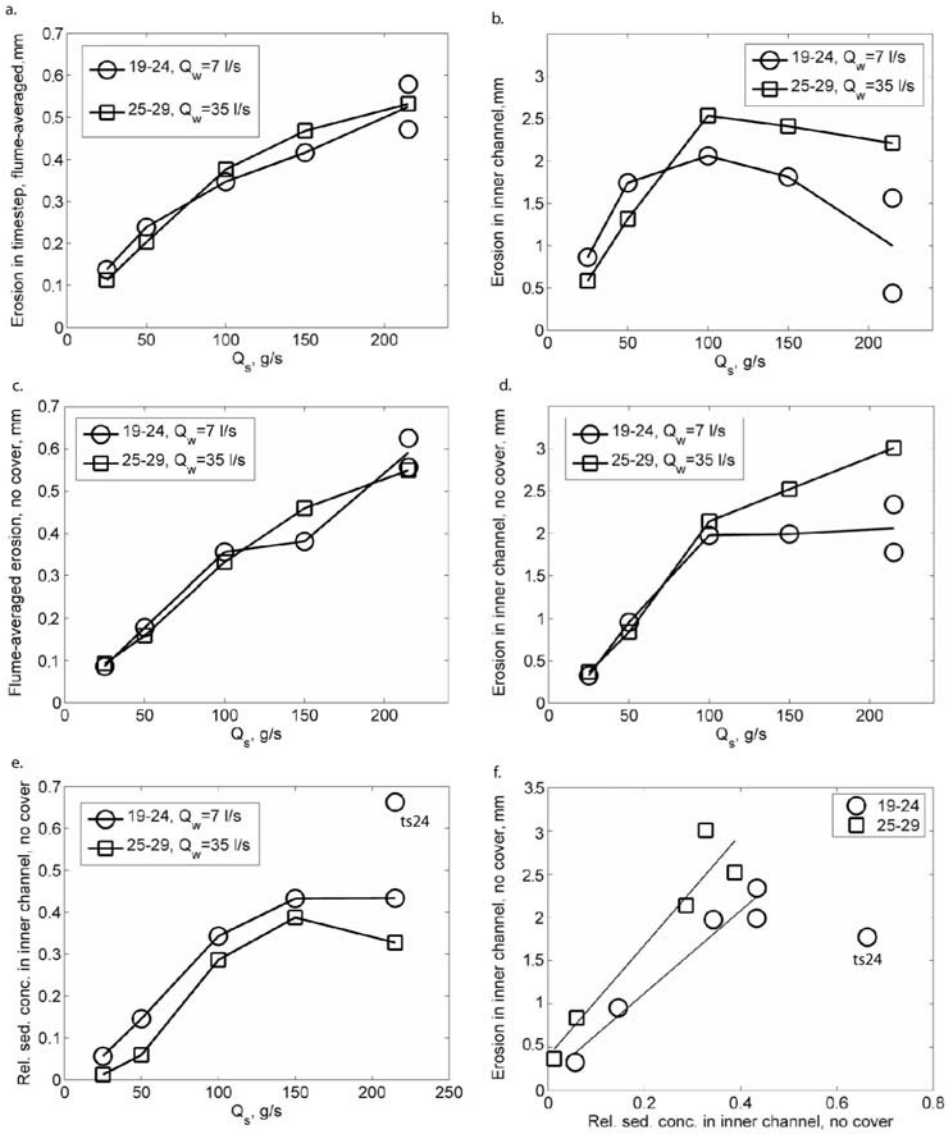

Figure 6. Erosion as a function of sediment flux for experiment A for time steps with variable sediment flux and constant discharge. All measurements of inner channel erosion and relative sediment concentration were made over a fixed width of 10 mm, following the inner channel centerline (e.g., Figures 1, 2, and 3). (a) Erosion per 15 min time step averaged over the large subset of flume area shown in Figures 1–3. Linear regressions (not shown) to time steps 19–24 and 25–29 have $R^2 = 0.93$ and 0.94, respectively, and the residuals are clearly nonrandom. (b) Erosion averaged along the axis of the inner channel per time step. Inner channel erosion rates are much higher than flume-averaged values. (c) Erosion averaged over the flume width, but only using the subset of longitudinal distances with no mapped alluvial cover (e.g., Figures 3 and 5). These relations are more linear than Figure 6a (R^2 = 0.96 and 0.97 for time steps 19–24 and 25–29, respectively, regressions not shown), and residuals are more randomly distributed. (d) Erosion along the inner channel axis, calculated from the same subset of longitudinal reaches with no alluvial cover as in Figure 6c. (e) Relative sediment concentration along the inner channel calculated from the same subset of longitudinal reaches with no alluvial cover as in Figures 6c and 6d. (f) Inner channel erosion for reaches with no alluvial cover plotted against relative sediment concentration also calculated for cover-free inner channel reaches. The relations are reasonably linear (R^2 = 0.96 for time steps 19–23, and R^2 = 0.92 for 25–29). Justifications for omitting time step 24 from the regression are discussed in the text.

Figures 6a and 6b are internally consistent because in 6a, the width of the zone of active sediment transport and incision (both on the inner channel sides and outside of the inner channel) increased with Q_s, increasing erosion outside of the inner channel and overwhelming the decrease in inner channel erosion due to increasing inner channel cover. In 6b, because we measured inner channel erosion over a fixed width narrower than the zone of active transport (e.g., Figure 4), the erosion rates reflect tools and cover effects without the additional degree of freedom provided by the topography-controlled width adjustment. Figure 6c again shows flume-averaged erosion rates, but this time calculated using only the subset of longitudinal distance categorized as having no deposition (cover). The relation between Q_s and erosion is more linear in 6c than 6a, as demonstrated by R^2 values for linear regressions (given in caption).

[29] Local erosion depends on local conditions at the bed. Figure 6d shows that for the subset of longitudinal distance along the inner channel centerline with no deposition, inner channel erosion (again, measured over a 10 mm fixed width) increases at low Q_s but then stabilizes. Inner channel erosion rates depend on the local sediment flux at the bed (designated as q_s^{loc}), rather than flume total Q_s. We assume that relative sediment concentration (e.g., Figure 2) is a reasonable proxy for q_s^{loc}. Figure 6e shows that relative sediment concentration along the inner channel does not increase uniformly with Q_s: at low total sediment flux the inner channel sediment concentration increases linearly with Q_s, but then "saturates" as sediment spreads laterally and the zone of active transport widens beyond the inner channel (Figures 6e, 4, and 2). Figure 6f shows cover-free inner channel erosion plotted against relative sediment concentration, suggesting that local erosion rate depends linearly on q_s^{loc}. We note that inner channel relative sediment concentration for time step 24 plots as an outlier (Figures 6e and 6f) for understood reasons, which also illustrate the importance of evolving bed topography and roughness as a control in these experiments. Time step 24 has high relative sediment concentrations along the inner channel, relative to previous time steps, as a result of increased incision and deepening of the upstream inner channel between time steps 19 and 24 (7.5 mm of mean inner channel lowering upstream of 200 cm; Figures 1 and 3). More sediment filled the upstream inner channel in time step 24 compared to 19 even though Q_s was the same (Figure 2). We discuss the effects of changing bed topography and roughness in sections 3.4 and 4.2. Nonetheless, Figure 6f indicates that local erosion rate increases linearly with local sediment flux right up to the onset of local deposition. Figure 6c similarly indicates a first-order linear trend between sediment flux and erosion rate in the absence of static alluvial cover.

3.3. Erosion Dependence on Discharge

[30] To isolate the dependence of erosion rate on discharge and on basal shear stress, we conducted three series of time steps (7–12, 13–18, 30–34) in which discharge was varied by an order of magnitude (7 l/s to 80 l/s) while sediment flux was held constant (Table 1). It is well known that flow depth, and thus shear stress, is nonlinearly related to fluid discharge. Accordingly we calculate in section 4.2 that the ~10x change in discharge resulted in a factor of four change in flume-averaged shear stress τ.

[31] In spite of an order-of-magnitude change in discharge, little variation in either the magnitude or spatial distribution of erosion was observed for time steps 13–18 (Figure 7). We find no consistent dependence of erosion rate on discharge, provided that alluvial cover does not change (Figure 8). Time steps 7–12 (2.7 mm sediment) and 13–18 (5.5 mm sediment) had zero cover. In contrast, time steps 30–34 had variable alluvial cover and show a positive discharge dependence on erosion (Figure 8). However, no dependence of erosion on discharge is observed for time steps 30–34 when erosion is calculated using only cover-free longitudinal reaches. Erosion rates were higher with the 5.5 mm gravel (13–18, 30–34) than with the 2.7 mm sediment (7–12), but the inner channel topography was also developing and may explain the greater erosion rates during later time steps [*Johnson and Whipple*, 2007]. We did not collect sufficient data to further evaluate possible controls of grain size on bed load erosion rate. Note that bed topography and roughness evolved during the compared time steps but apparently did not affect the relationship between flume-averaged erosion and discharge, beyond influencing alluvial deposition. Finally, Figure 6 also demonstrates that erosion rates varied with sediment flux but not with discharge: over a wide range of bed load flux, the overlapping data sets for $Q_w = 7$ and $Q_w = 35$ indicate that flume-averaged erosion rates do not depend on discharge.

3.4. Bed Roughness Evolution

[32] Bed roughness increased during these experiments as the relatively planar initial bed was incised by nonuniform erosion. Figure 9a shows the evolution of the inner channel longitudinal topography (i.e., following the centerline of the inner channel) of experiment A (variable sediment flux and discharge). The inset plot shows a subset of the same profiles with no vertical exaggeration, to emphasize that incision was strongly focused on upstream-facing surfaces. The vertical incision rate is only ~1/5 of the downstream migration rate of the bedrock crests and troughs. We have observed erosional "bedforms" in natural bedrock channels in a variety of field settings that share morphologic similarities to the experimental crests and troughs, suggesting that their development is not unique to our experiments (Figure 9b). Figure 9c shows the relation between inner channel longitudinal topography and erosion rate for time step 21. In reaches without alluvial cover (i.e., upstream of 225 cm), local erosion rate maxima occur on upstream faces, and minima occur on downstream faces. The development of inner channel longitudinal topography and patterns of erosion were similar in experiment B (constant Q_w, Q_s; data not shown).

[33] Consistent with *Johnson and Whipple* [2007] and *Finnegan et al.* [2007], we characterize bed "roughness" as the standard deviation of surface elevations, detrended longitudinally to remove the average flume slope. This simple measure of roughness is equivalently called interface width, and has been used in a variety of disciplines to quantify changes in surface topography [*Barabasi and Stanley*, 1995]. Figure 10 shows how both flume-averaged roughness (the standard deviation of all surface elevations) and inner channel roughness (standard deviation of the inner

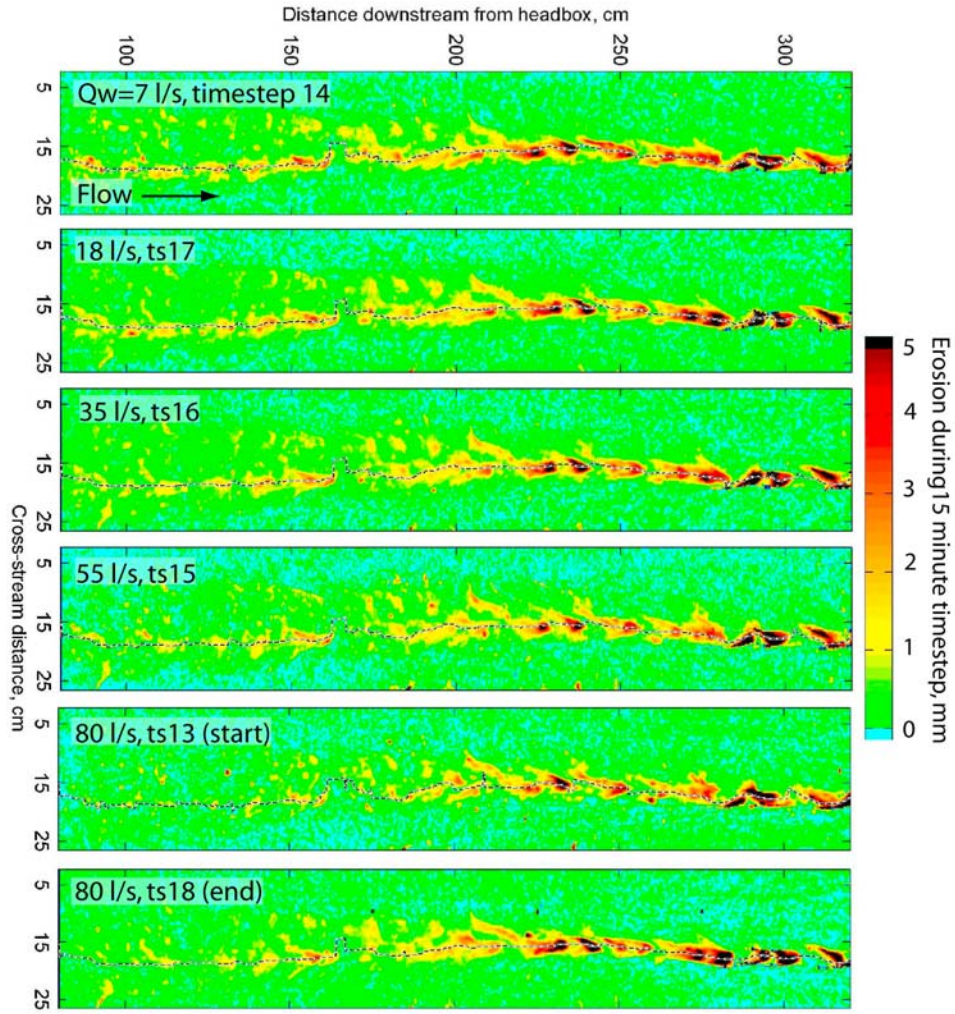

Figure 7. Erosion in time steps with constant Q_s (100 g/s, 5.5 mm) and variable Q_w. Little change in either erosion rate or pattern is seen over a tenfold change in discharge. Inner channel centerlines are indicated.

channel longitudinal elevations) changed during experiments A and B. The progressive increase in flume-averaged roughness during both experiments largely reflects inner channel downcutting as the upper bed surface remained minimally abraded.

[34] Increasing inner channel roughness primarily reflects the lowering of troughs relative to crests. Inner channel roughness in experiment A increases until the initiation of alluvial cover (starting in time step 19), suggesting that a roughness-dependent threshold for alluviation may have been reached. However, once local cover was present on the bed the inner channel roughness decreased slightly but remained relatively constant (Figure 10a), even as the overall inner channel continued to incise. Figure 9c indicates how variations in alluvial cover limited the growth of inner channel topography: in reaches where cover was present (225–320 cm downstream), erosion was focused on topographic highs (crests) and strongly inhibited in topographic lows (troughs) and the lower portions of upstream faces. Cover tends to fill local topographic lows, while the local zone of active sediment transport becomes elevated by deposition below. Therefore, Figure 10a suggests that variations in sediment flux and transport capacity in experiment A limited the growth of bed roughness along the inner channel. This is the longitudinal equivalent of the lateral erosion pattern in Figures 3 and 4, which shows that variations in cover similarly focused transport and erosion at different elevations.

[35] In contrast, in experiment B (constant Q_w, Q_s in all time steps), inner channel roughness never stabilized (Figure 10b). The amplitude of inner channel "bedforms" continued to grow as upstream faces migrated downstream while the forms also deepened. After the time steps shown, trough downcutting became limited by the base of the flume. Presumably alluviation would have eventually occurred in experiment B and acted as a negative feedback on continued downcutting had the bottom not been reached. In the discussion section we interpret feedbacks between alluvial cover and roughness, and find that roughness increases the

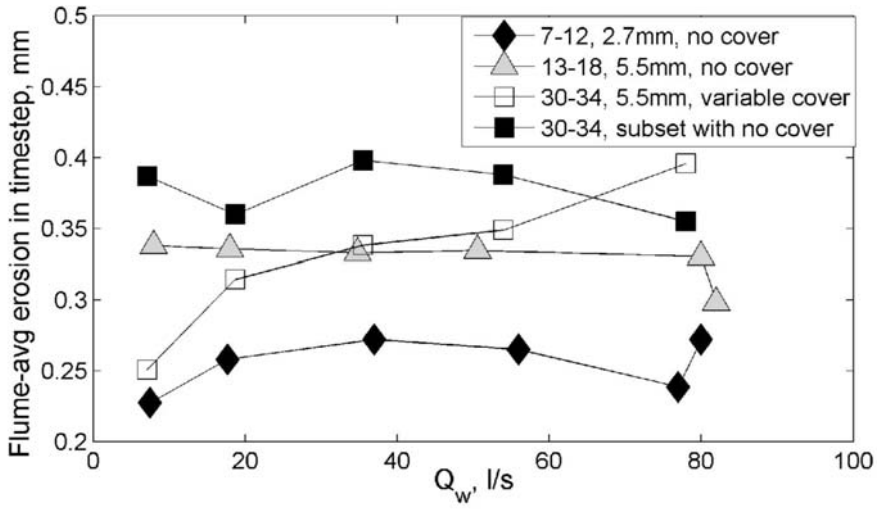

Figure 8. Flume-averaged erosion (i.e., the average vertical distance of bed lowering that occurred during each 15 min time step) plotted against discharge. Time steps 7–12 and 13–18 have no alluvial bed cover in any of the time steps and show no significant dependence of erosion on discharge. Time steps 30–34 have some cover in all but the highest discharge time step. When erosion is calculated for time steps 30–34 from longitudinal zones with no cover, erosion shows no dependence on discharge.

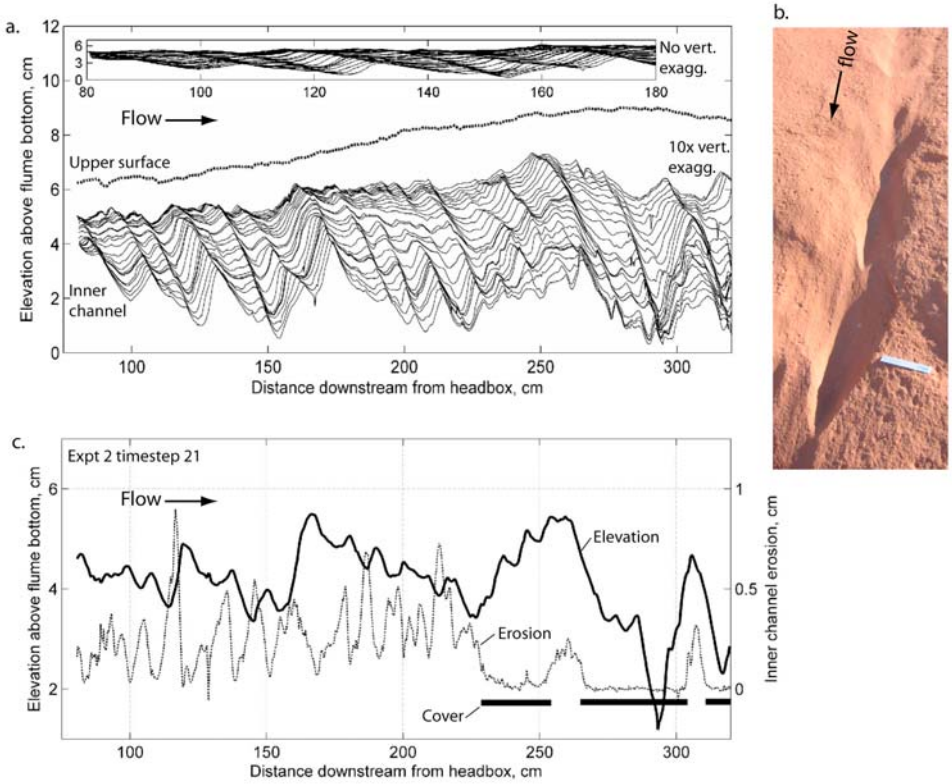

Figure 9. (a) Inner channel longitudinal topography, time steps 6–34. Vertical exaggeration is ~10x. The long inset plot shows a subset of the data with no vertical exaggeration. (b) Field photograph of a bedrock channel with similar erosional forms to the crests and troughs developed in the flume experiment. The ruler is 15 cm long. The field location is near Bullfrog, Utah, and the bedrock is Navajo sandstone. (c) Topography and erosion for experiment A time step 21, showing erosion focused on upstream slopes and alluvial cover inhibiting erosion.

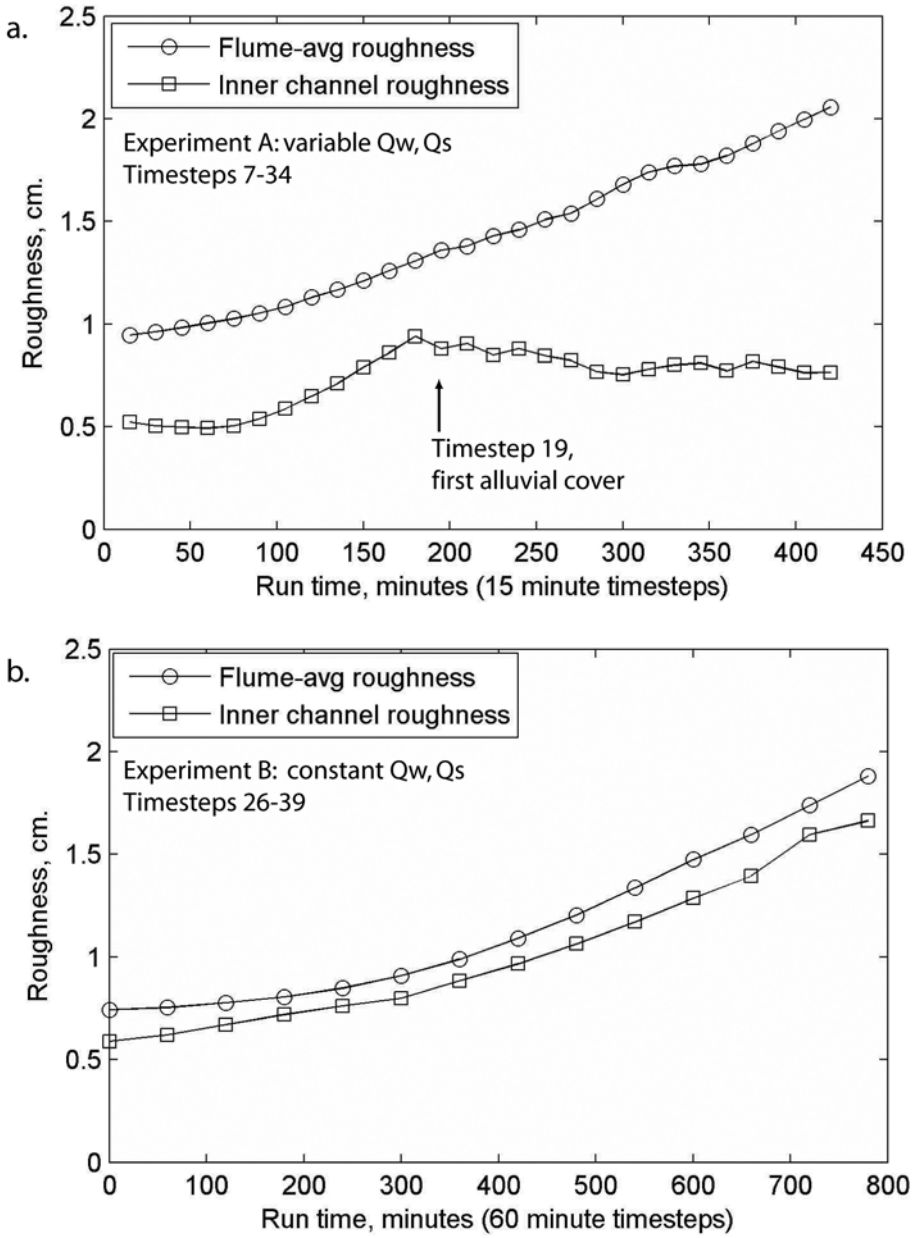

Figure 10. Bed roughness (standard deviation of bed elevations) calculated for the entire bed surface and also for the longitudinal inner channel topography. (a) Experiment A. (b) Experiment B, eroded with constant Q_w and Q_s in all time steps. Flume-averaged roughness (which largely reflects inner channel downcutting) developed similarly to experiment A, but no bed cover was present in this experiment and inner channel roughness did not stabilize.

potential for alluvial cover, while cover can limit bed roughness development.

4. Discussion

[36] Under the conditions of these experiments, we found that (1) erosion rate increased linearly with sediment flux; (2) erosion rate was not explicitly dependent on discharge or flume-averaged shear stress, independent of changes in sediment flux and cover; (3) bed cover increased approximately linearly with Q_s at a given discharge, once thresholds of Q_s and bed roughness were overcome; (4) flume-averaged erosion rate decreased linearly with the extent of alluvial bed cover; and (5) variability in discharge and sediment flux limited the growth of bed roughness by changing the spatial distribution of local alluviation and erosion. Within experiment A (which we primarily discuss), we conducted multiple sets of time steps (7–12, 13–18, 19–24, 25–29, 30–34) in which either sediment flux or discharge were held constant while the other was systematically varied (Table 1).

[37] Our experimental method allowed us to isolate, to a large extent, key relations between factors that strongly covary in nature: erosion rate, sediment flux, alluvial cover,

bed roughness and discharge. We set the initial channel slope, independently controlled sediment flux and discharge, and allowed erosion to occur. Rather than imposing an unrealistic bed topography (e.g., an entirely planar surface), a benefit of our approach is that the bed topography was allowed to evolve "naturally" (i.e., under the imposed set of conditions), thus capturing feedbacks between differential erosion, local bed topography, local sediment flux and shear stress. However, the evolving bed topography was also a limitation, because the bed topography changed somewhat within sets of time steps that we compare. Our analysis generally assumes that the change in topography (e.g., between time steps 19 and 24) was minor compared to the variations in external forcing (e.g., sediment flux or discharge), and that the primary effect of the topographic adjustment was to introduce noise to the data (e.g., in Figures 5, 6, and 8).

[38] Erosion was driven by the strongly disequilibrated conditions of a high bed slope, high shear stress and sediment flux lower than the overall transport capacity of the flow. The relatively planar initial bed surface gradually developed an initial channel, as a morphological response to the disequilibrated conditions. Because Q_w and Q_s were intentionally changed between each time step of experiment A, the resulting channel morphology at the end of the experiment reflected an averaging of variable forcing. As the channel morphology was intentionally not allowed to fully equilibrate to the imposed external forcing, our experiments do not capture channel adjustment in its entirety.

[39] Instead, in comparing erosion rates within steps of time steps with systematic variations in forcing, we again make the assumption that the minor amount of bed adjustment within time step series was not sufficient to substantially change the degree of channel disequilibrium. Experiments by *Johnson and Whipple* [2007] and *Finnegan et al.* [2007] allowed bedrock channel morphology to adjust to nearly equilibrated conditions. *Johnson and Whipple* [2007] interpret that the formation of an inner channel may indicate that the overall channel is sediment starved (i.e., $Q_s/Q_t < 1$), but found that bed morphology eventually adjusted under constant forcing such that $q_s^{loc} \sim q_t^{loc}$ along the inner channel, where q_t^{loc} is the local transport capacity over a given subsection of bed area, such as along the inner channel. *Finnegan et al.* [2007] held imposed Q_s and Q_w constant in different time steps, and let erosion run until the topography equilibrated to a condition with $q_s^{loc} \sim q_t^{loc}$ and essentially continuous bed cover in their inner channels. Their decreasing erosion rates reflected a gradual transition to alluvial cover-dominated conditions, consistent with the findings of *Johnson and Whipple* [2007].

[40] Equations (1) and (4) introduced key components of several sediment flux–dependent bedrock incision models, parameterized with three basic terms: sediment flux, bedrock exposure and shear stress. We interpret our experimental results within this model framework and evaluate proposed relations for these terms.

4.1. Sediment Flux Term: $E \propto Q_s$

[41] We found that erosion rate scaled essentially linearly with sediment flux in the absence of alluvial cover, consistent with the tools effect as formulated in the saltation-abrasion model [*Sklar and Dietrich*, 2004]. This was true for both the flume-averaged case where erosion rate depended on total sediment flux (Q_s), and also for inner channel erosion where incision rate depended on local sediment flux (q_s^{loc}) (Figure 6). In the flume-averaged case, the width of the zone of active sediment transport and hence the width of erosion increases with Q_s. These data are consistent with experiments of *Finnegan et al.* [2007], who observed that inner channel width scaled with sediment flux. They found that the vertical incision rate of the inner channel did not vary with total sediment flux, but that the width of the inner channel adjusted, and hypothesized that the local sediment concentration adjusted to a constant value. In our experiments we measured the inner channel sediment concentration (Figures 2, 4, and 6), supporting the hypothesis of *Finnegan et al.* [2007] and confirming the q_s^{loc} dependence of local erosion rate.

4.2. Shear Stress Term: $E \propto (\tau/\tau_{cr} - 1)^a$

[42] Figure 8 shows that we found no explicit dependence of flume-averaged bed load erosion rate over an order-of-magnitude variation in discharge, provided that sediment flux and static alluvial cover remained constant. In this section we calculate flume-averaged basal shear stress τ, and find a factor of four variation in τ as a result of the factor of 10 variation in imposed discharge. Our experimental design allowed us to largely isolate shear stress from both sediment flux and alluvial cover, even though these factors strongly covary in nature. However, an important limitation of our method is that we only can calculate flume-averaged shear stresses, and do not have constraints on local shear stresses (e.g., along the inner channel). The flume-averaged basal shear stress τ was calculated for each time step assuming steady, uniform flow:

$$\tau = \rho_w g R S_w, \tag{5}$$

where ρ_w is water density (1000 kg/m^3), g is gravitational acceleration (9.81 m/s^2), R is hydraulic radius (flow cross-sectional area/wetted perimeter distance, m) and S_w is the water surface slope (calculated from measured water depths and bed slopes). We calculate R in each time step based on measured flow depths and the evolving surface topography. Corrections to the basal shear stress were made to account for the partitioning of some stress on the flume walls. We note that shear stress was varied by changing discharge rather than slope. *Chatanantavet and Parker* [2006] isolated the effects of bed slope and shear stress, and found an explicit slope-dependent control in which erosion rates increased with bed slope, while holding shear stress constant (by varying slope). They also found that saltation trajectories were explicitly sensitive to channel slope, not just fluid shear stress. While not addressed in our experiments, there may be explicit slope-dependent controls on bedrock abrasion that cannot be accommodated solely by parameterizing the influence of bed slope in terms of fluid shear stress.

[43] Equations (1) and (4) introduced a general bedrock incision model with possible different power law dependencies on shear stress, in the form $E \propto (\tau/\tau_{cr} - 1)^a$. Figure 11 shows flume-averaged erosion data for each set of time steps with variable discharge and constant sediment flux (7–12; 13–18; 30–34; Figure 8) plotted as a function of flume-averaged excess shear stress, $\tau/\tau_{cr} - 1$. Erosion data

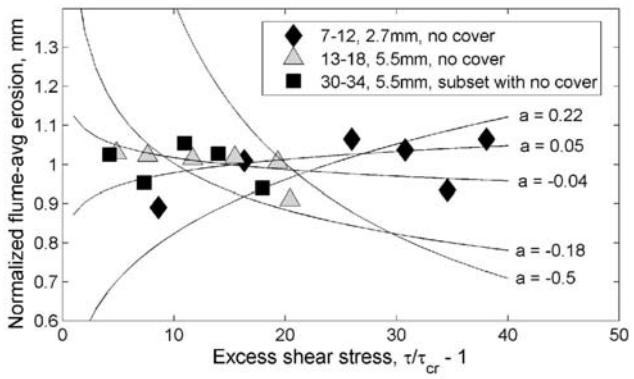

Figure 11. Flume-averaged erosion, normalized by the mean erosion in each set of time steps (7–12, 13–18, 30–34), plotted against excess shear stress (calculated for τ_{cr} = 0.03). These time steps have variable discharge and constant sediment flux (Figure 8). Power law regressions to constrain excess shear stress exponent a (equations (1) and (4)) are shown and described in the text. The minimum 95% confidence a value (−0.18) is a fit to time steps 30–34, while the maximum (a = 0.22) is a fit to time steps 7–12. The saltation-abrasion model exponent, a = −0.5, is shown for reference.

for each set of time steps was normalized by the mean of those time steps, highlighting that erosion rate is independent of excess shear stress in our data set.

[44] We constrain a with our experimental data with linear regressions of $\log(\tau/\tau_{cr} - 1)$ against $\log(E)$ (Figure 11). When the three time step series with variable Q_w and constant Q_s are fit separately, at 95% confidence a ranges between −0.18 and +0.22. Importantly, all three regressions predict a values within error of zero ($p > 0.05$). When all three time step series are normalized to the same mean erosion value and regressed together, the larger number of regressed data points over a greater range of excess shear stress constrain a to fall between −0.04 and 0.05 at 95% confidence. The saltation-abrasion model predicts a = −0.5 [*Sklar and Dietrich*, 2004], the *Chatanantavet and Parker* [2009] model predicts a = 0, and the shear stress incision model predicted $a \geq 1$ [*Howard and Kerby*, 1983; *Whipple and Tucker*, 1999]. Therefore, the shear stress exponent $a \approx 0$ and the *Chatanantavet and Parker* [2009] formulation of sediment-dependent erosion are most consistent with our results.

[45] We assumed in the above analysis that τ^*_{cr} = 0.03 (where τ^*_{cr} is the critical Shields stress for initiation of motion, $\tau^*_{cr} = \tau_{cr}/(\rho_s - \rho_w)gD$, with ρ_s sediment density and D median sediment grain diameter), to be consistent with *Sklar and Dietrich* [2004]. We did not experimentally measure τ^*_{cr}, and acknowledge that factors including sediment packing density on the bed [e.g., *Dancey et al.*, 2002] and bed slope influence local values of τ^*_{cr}. *Lamb et al.* [2008] show a wide range of compiled values for experimental and field τ^*_{cr}, with most data falling between 0.03 and 0.06. Using τ^*_{cr} = 0.06 reduces the calculated values of excess shear stress approximately in half (to a range from 1.6 to 18.6), but changes the regression constraints on a by only a small amount to be more tightly constrained to between −0.16 and 0.21 when regressed separately, or between −0.04 and 0.04 when regressed together.

[46] Mechanistically, it is difficult to interpret exactly what the lack of shear stress dependence of erosion means, because our calculations only give flume-averaged measurements of shear stress rather than local measurements along the inner channel where much of the erosion was focused. We present two hypotheses to explain the lack of erosional dependence on shear stress: first, that the bed topography effectively decoupled local shear stresses along the zone of active sediment transport from flume-averaged shear stresses, and second, that both local bed topography and saltation hop lengths influenced the rate and intensity of sediment impacts on the bed. These two hypotheses are evaluated in the following sections.

4.2.1. Topographic Decoupling of Local and Average Shear Stress

[47] The first hypothesis is that the rough bed topography effectively decoupled local bed shear stresses from the flume-averaged values, particularly along the zone of active transport (primarily the evolving inner channel). If true, it is possible that local erosion does depend directly on local shear stress (either positively or negatively), but that this effect was overwhelmed in our experiments by the rough bed topography. If so, a similar effective decoupling may be prevalent in many natural bedrock channels. We think it likely that, as the inner channel deepened, shear stresses at the inner channel bottom did become less sensitive to the overall discharge. However, we doubt that the topography-controlled decoupling of local and flume-averaged shear stress was so complete that it can entirely account for the lack of erosion dependence on discharge, for two reasons: First, in the initial bed load time steps (7–12), the bed topography was broadly lower in the middle of the flume but did not yet have a well-defined inner channel (Figure 1), and the overall bed roughness in these time steps was relatively low (Figure 10), making it unlikely that decoupling between mean and local shear stress would be complete or even strong at this stage in the bed evolution. Second, alluvial cover varied in the inner channel in time steps 30–34 from 0% at the highest discharge to 51% at the lowest discharge while imposed sediment flux remained the same, implying that shear stress did vary at the bottom of the inner channel even at the end of the experiment, when the inner channel was deepest. Therefore, we doubt that the observed lack erosion dependence on shear stress was entirely a result of our particular bed topography. These two arguments also suggest that the lack of correlation between channel-averaged shear stress and channel-averaged erosion may be robust over a fairly wide range of bed topographies and roughnesses, provided again that other variables (sediment flux, cover) remain constant.

4.2.2. Saltation Trajectory Scalings and Bed Topography

[48] A second hypothesis to explain the lack of correlation between shear stress and erosion is that both saltation trajectories (controlled by shear stress) and bed topography influence the rate and intensity of particle impacts on the bed. We expand on the saltation-abrasion model and propose two alternate scaling relations between erosion and excess shear stress (i.e., exponent a). While none of these scalings are directly consistent with our data, we present

them (1) to interpret what the lack of erosional dependence on shear stress could mean physically, (2) to show that a wide range of scalings between erosion and shear stress are plausible as a result of bed roughness effects, and (3) because many bedrock incision models have been framed in terms of a shear stress dependence. *Sklar and Dietrich* [2004] derived $a = -0.5$ by mechanistically parameterizing E in terms of the kinetic energy of particle impacts and the distance between impacts:

$$E \propto \frac{u_\perp^2}{L_s}, \tag{6}$$

where $u_\perp$ is the component of the particle impact velocity perpendicular to the local bed and L_s is the saltation hop length. A key assumption in (6) is that the bedrock bed remains perfectly planar as it erodes. Because the bed is planar, $u_\perp$ equals the vertical velocity of a particle settling in still water from saltation hop height H_s. *Sklar and Dietrich* [2004] calculate $u_\perp$ as H_s divided by the descent time:

$$u_\perp \propto \frac{H_s u_s}{L_s}, \tag{7}$$

where u_s is the average horizontal component of particle velocity. Finally, *Sklar and Dietrich* [2004] find the following empirical relations between excess shear stress and saltation trajectory components based on published studies:

$$H_s = 1.4D\left(\frac{\tau^*}{\tau_{cr}^*} - 1\right)^{0.5}, \tag{8}$$

$$L_s = 8.0D\left(\frac{\tau^*}{\tau_{cr}^*} - 1\right)^{0.88}, \tag{9}$$

$$u_s = 1.56\sqrt{R_b g D}\left(\frac{\tau^*}{\tau_{cr}^*} - 1\right)^{0.56}, \tag{10}$$

where R_b is $\rho_s/\rho_w - 1$. Combining (6) through (10) results in the saltation-abrasion model scaling of excess shear stress:

$$E \propto \left(\frac{\tau^*}{\tau_{cr}^*} - 1\right)^{-0.52}, \tag{11}$$

reflecting a stronger variation in L_s than $u_\perp$ with excess shear stress. Exponent a is rounded to -0.5 for the purpose of discussion.

[49] However, settling velocity may not be the appropriate parameterization of $u_\perp$ as bed roughness develops. As erosional bed topography becomes complex, we hypothesize that $u_\perp$ may scale with the horizontal component of particle velocity u_s rather than particle settling velocity because particles will impact the bed on upstream-facing surfaces with a horizontal velocity component. If saltation hop lengths still control particle impact rates, erosion rate should scale as

$$E \propto \frac{u_s^2}{L_s} \propto \left(\frac{\tau^*}{\tau_{cr}^*} - 1\right)^{0.24}. \tag{12}$$

Note the weak positive dependence on excess shear stress ($a = 0.24$).

[50] As bed topography becomes more complex and roughness continues to increase, particles may impact the variable bed topography at rates not controlled by particle trajectories – the physical roughness length scale, rather than saltation hop lengths, may determine the frequency of bed impacts. In this regime, erosion by bed load erosion may be highly localized but should scale with the square of particle velocity, leading to a stronger dependence of erosion rate on shear stress:

$$E \propto u_s^2 \propto \left(\frac{\tau^*}{\tau_{cr}^*} - 1\right)^{1.12}. \tag{13}$$

Equation (12) ($a = 0.24$) is closer to the scaling from our data ($a \approx 0$) than either the saltation-abrasion model ($a = -0.5$) or equation (13) ($a = 1.12$). If the above scalings between excess shear stress, particle trajectories, bed roughness and erosion are physically reasonable, we interpret that the frequency of particle impacts was influenced by saltation trajectories but that perpendicular impact velocities scaled with the downstream velocities of the particles, rather than with particle descent velocity (equation (12)). We also note that a relatively minor change in exponents can make the above framework of scaling relationships match our data: a scaling of $E \propto u_s^{1.5}/L_s$ gives $E \propto (\tau/\tau_{cr} - 1)^{-0.04}$, which for example could indicate a bed roughness-dependent reduction in near-bed flow and particle velocity relative to that predicted by equation (10) over a planar bed.

[51] Calculations suggest that "normal" saltation trajectories may be physically plausible over the rough beds that developed in our experiments. For 5.5 mm sediment, equation (8) gives hop heights of ~16 mm and ~34 mm for $\tau/\tau_{cr} - 1$ of 4 and 19, respectively. Because our measure of bed roughness is the 1σ standard deviation of inner channel elevations, the maximum inner channel roughness of ~8 mm (i.e., $\pm 2\sigma$ spans 32 mm) in experiment A is comparable to the calculated saltation heights. Similarly, equation (9) gives saltation hop lengths of ~150 mm to ~600 mm for $\tau/\tau_{cr} - 1$ of 4 to 19, respectively. The spacing of inner channel crests and upstream faces averages to ~150–250 mm (Figure 9). Thus, the amplitude and wavelength of bed roughness are comparable to calculated saltation length scales, consistent with the interpretation that bed topography and sediment trajectories play opposing roles in minimizing the dependence of impact wear on shear stress.

[52] We have a direct constraint on the distribution and intensity of particle bed impacts: The downstream migration of "bed forms" (Figure 9) demonstrates that most impacts, or at least the impacts that cause the most erosion, occur on upstream faces. Particle impacts on sloping faces will be less oblique than over a truly planar bed, consistent with $u_\perp$ scaling more closely with u_s than with settling velocity. Note also that the bed roughness that developed is not an independent feature of the bed, but was a result of focused erosion. Positive feedbacks between the localization of particle impact rates and intensities and the bed topography led to the development of the stable migrating bed forms. However, the observation that minimal shear stress dependence on erosion occurs over a wide range of bed roughness

suggests that erosion rate may be less sensitive to the details and amplitude of bed topography once a small amount of roughness exists.

[53] By using two sediment sizes the experimental conditions span most of the excess shear stress range of bed load transport (Figure 11), consistent with our qualitative observations of transport by saltation. A criteria for computing the mode of sediment transport (e.g., bed load transitioning to suspended load) is the Rouse number, w_s/ku_*, where w_s is settling velocity, $u_* = \sqrt{\tau/\rho_w}$ is shear velocity, and $k = 0.4$ is Von Karman's constant. For Rouse number > 2.5 particles should be entirely bed load because the settling velocity is larger than the strength of turbulent fluctuations which scale with shear velocity [*Rouse*, 1937; *Nino et al.*, 2003; *Sklar and Dietrich*, 2004]. In our experiments this condition corresponds to $\tau/\tau_{cr} < \sim 40$ for $\tau_{cr} = 0.03$ (as shown in Figure 11) or $\tau/\tau_{cr} < \sim 20$ for $\tau_{cr} = 0.06$, for both grain sizes used, confirming bed load transport conditions.

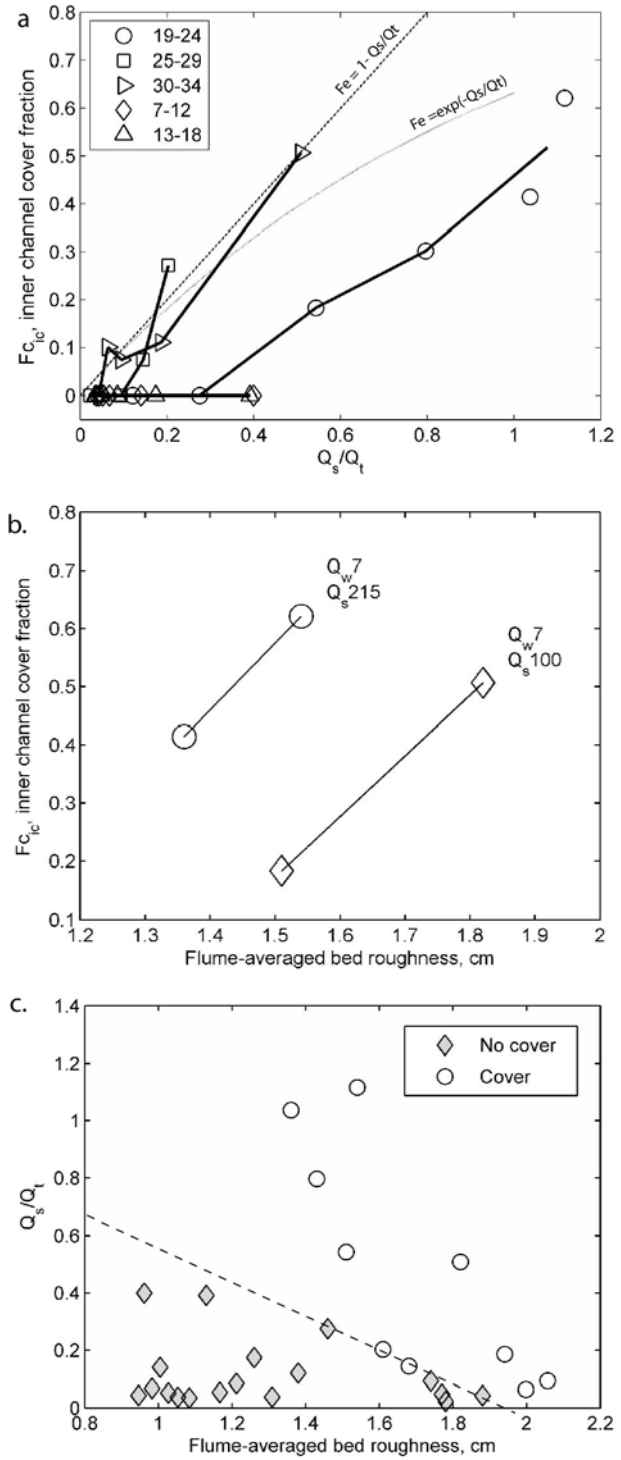

4.3. Cover Term ($Fe = 1 - Q_s/Q_t$) and Bed Roughness

[54] Figures 3 and 5 indicate that static alluvium covered a small portion of the entire flume bed area, but a substantial fraction of the inner channel. Sediment flux, sediment transport capacity (Q_t) and bed topography all controlled the extent and patterns of alluvial cover. As highlighted above, we only have flume-averaged rather than local measurements of τ. Following *Sklar and Dietrich* [2004], we calculate flume-averaged Q_t using the *Fernandez Luque and van Beek* [1976] relation:

$$Q_t = 5.7 w \rho_s \left(R_b g D^3\right)^{1/2} \left(\tau^* - \tau^*_{cr}\right)^{3/2}, \qquad (14)$$

where R_b is $\rho_s/\rho_w - 1$, w is flume width, Shields stress $\tau^* = \tau/((\rho_s - \rho_w)gD)$, and we assume $\tau_{cr}^* = 0.03$. Because τ^* was flume averaged, Q_t also represents a flume-averaged capacity and may only approximately represent local transport capacities (q_t^{loc}). Shear stress calculations also assumed a bare bedrock bed (used to calculate hydraulic radius from topographic scans), and neglected the presence of both static deposits and active bed load transport which would also influence local shear stresses.

[55] Alluvial cover along the inner channel increases with Q_s/Q_t (Figure 12a). There is a similar positive correlation between Q_s/Q_t and total bed cover fraction (Fc_{tot}) and active bed cover fraction (Fc_{act}), although as in Figure 5 the actual values of cover fraction are different (plots not shown). Note that Q_s/Q_t was calculated to be slightly higher than 1 for time steps 19 and 24, perhaps because at low Q_w the flow across the zone of active transport was somewhat deeper

Figure 12. (a) The fraction of distance along the inner channel centerline with alluvial cover plotted as a function of Q_s/Q_t for all experiment A time steps (7–34). Table 1 gives conditions for the different time step series. Time steps 7–18 had zero cover. Time steps 19–24 suggest that a threshold value of Q_s/Q_t must be reached before alluviation initiates (Figure 11a). Earlier time steps (7–18) developed no cover even though they span the same range of Q_s/Q_t with cover in later time steps. Also shown are the linear saltation-abrasion model cover relation (equation (2)) and the exponential cover relation of *Turowski et al.* [2007b] (equation (3)). (b) Alluvial cover plotted as a function of flume-averaged roughness. (c) Plot of flume-averaged bed roughness against Q_s/Q_t for all time steps, with points classified as either having or not having alluvial cover. An increase in either roughness or Q_s/Q_t will increase alluvial cover. The dotted line was positioned visually and is not statistically meaningful as a discriminator between the data fields.

than the average depth and local shear stresses were probably higher than calculated. Both the linear and exponential cover models (equations (2) and (3)) predict increasing cover with Q_s/Q_t, and our data are not sufficient to rigorously differentiate between these models. Rather, our data demonstrate that bed topography makes the relation between flume-averaged Q_s/Q_t and cover fraction nonunique. Experimental results by *Chatanantavet and Parker* [2008] similarly are consistent with a linear relation (equation (2)), but the variability due in part to bed roughness controls in both their and our data are larger than the differences between the linear and exponential models.

[56] In early time steps (7–18) no deposition occurred (Figure 12a). In time steps 19–24 Q_s/Q_t-dependent deposition did occur, but at lower cover fractions than for time steps 25–34. Because we do not have measurements of local transport capacities, we cannot constrain particular values of q_s^{loc}/q_t^{loc} that may be thresholds for deposition. Nonetheless, Figure 12a suggests that a threshold value of q_s^{loc}/q_t^{loc} was required for local deposition to occur. As incision progressed and overall bed roughness increased, q_t^{loc} at the bottom of the inner channel decreased, leading to threshold-dependent cover.

[57] Cover increases with flume-averaged roughness, all other variables held constant (Figure 12b). Two sets of external forcing conditions (Q_w = 7 l/s, Q_s = 100 and 215 g/s) had repeated points with sediment cover and show a consistent relationship between increasing bed roughness and increasing cover. Figure 12c shows that both bed roughness and Q_s/Q_t influence alluvial cover. Increasing bed roughness allows cover to develop for decreasing values of flume-averaged Q_s/Q_t.

[58] Bed topography likely influences cover effects in several ways in our experiments. First, local bed topography influences local bed load flux (q_s^{loc}) by channeling sediment through interconnected topographic lows: in our experiments, the inner channel. Second, bed topography is a strong control on local transport capacity, with local lows presumably having lower shear stresses than local highs. Topographically controlled variations in q_s^{loc} and q_t^{loc} can likely explain the nonuniform spatial patterns of alluvial cover observed. For example, in time step 19 the upstream ~60% of the inner channel was cover-free, while the downstream reach was nearly completely covered (Figure 3). While total sediment flux, discharge and transport capacity were the same in both halves, Figures 1 and 2 demonstrate for time step 19 that the inner channel downstream reach was both deeper and had higher relative sediment concentrations, suggesting that q_t^{loc} was lower and q_s^{loc} higher in the downstream reach, leading to deposition. The inner channel became deeper downstream (Figure 9a), and cover preferentially filled in topographic lows (Figure 9c). Another positive feedback with roughness may occur once alluviation initiates: deposits of gravel form a rougher local surface than the smoothly abraded concrete, further reducing local transport capacity and encouraging deposition [*Chatanantavet and Parker*, 2008].

[59] A third way that topography influences cover effects is that local alluvial deposition is greatly enhanced in some locations (such as along the naturally developed inner channel), but inhibited elsewhere (such as local highs, or in our experiments the bed area outside of the inner channel). Even when alluvial cover is present over some of the channel bed, the variable bed topography can lead to sediment transport and incision on other parts of the bed, as illustrated in Figure 4. In our experiments, the inner channel did not contain all of the sediment load at high Q_s, greatly increasing erosion outside of the inner channel. In this way, the presence of the inner channel reduced the efficiency of cover in inhibiting incision over the rest of the flume bed. Our measurements of cover over a rough bed topography with a naturally evolving inner channel complement experiments of *Chatanantavet and Parker* [2008], who imposed small-amplitude bed roughness on a nonerodible, essentially planar bed and measured the systematics of static deposition over the entire flume bottom. By the end of our experiments differential erosion had led to the development of much more overall roughness than studied by *Chatanantavet and Parker* [2008], and we in general observe much stronger bed roughness control on cover.

[60] In our set of experiments, several arguments suggest that static cover effects (stable alluvial deposition covering the local bed) are more important than the dynamic cover mechanism hypothesized by *Turowski et al.* [2007b], in which local erosion rates are reduced at high concentrations of moving bed load. First, Figures 6c and 6f show linear relations between sediment flux and erosion, even though the sediment fluxes were high enough for deposition to occur elsewhere along the inner channel. If dynamic cover was a strong inhibitor of incision, at high sediment flux one would expect erosion rate everywhere to decrease, or at least to increase much more slowly. Second, Figures 3 and 9c show that the transitions between eroding and noneroding locations are abrupt, which is more consistent with a sudden cessation of erosion once a threshold of static alluviation is crossed than with a gradual reduction in erosion rate as local sediment concentration increases. Similarly, Figures 2 and 3 indicate that erosion rates along the inner channel vary greatly due to cover effects, but inner channel relative sediment concentrations vary minimally (most apparent in comparing time steps 19, 21 and 23 downstream of ~215 cm from the head box). Dynamic cover would predict a reduction in erosion along the whole inner channel length, rather than abrupt variations in erosion rate. The interpretation that static cover effects are dominant would be stronger if we had been able to directly and independently quantify the zones with static alluvial cover, rather than interpreting cover based on the erosion maps. However, during the experiments we could visually observe static deposition underneath moving sediment in many of the zones mapped as cover.

[61] To summarize, our results are consistent with a gradual increase in cover fraction with increasing Q_s/Q_t over a wide range of Q_s/Q_t values, broadly consistent with both linear and exponential cover models (equations (2) and (3)). However, we also find strong control on cover fraction by the local bed topography. These interpretations should be further evaluated in channels with more uniformly distributed bed roughness [e.g., *Davis et al.*, 2005; *Chatanantavet and Parker*, 2008].

4.4. Magnitude-Frequency Relations and Application to Natural Channels

[62] Variability in discharge and sediment flux enabled inner channel bed roughness to stabilize even as the overall

inner channel continued to incise. The amplitude of inner channel bed topography in experiment A initially increased as the inner channel incised down, but then stabilized because alluvial cover filled topographic lows during some of the later time steps, focusing erosion on topographic highs along the inner channel (Figures 9c and 10a). Variability in alluvial cover was driven by imposed changes in discharge and sediment flux. In contrast, experiment B had constant Q_w and Q_s forcing, deposition did not occur, and inner channel bed roughness continued to increase throughout the experiment (Figure 10b). Our controlled experimental results are consistent with field studies of *Hartshorn et al.* [2002], *Turowski et al.* [2007a], and *Johnson et al.* [2010], who found through field monitoring of natural erosion that sediment mantling at lower bed elevations led to increased erosion rates at higher bed elevations. We interpret that a wide distribution of flood magnitudes and sediment supply rates may stabilize bed roughness in natural channels.

[63] Because our approach in these experiments was to systematically explore parameter space to observe how erosion by bed load is sensitive to Q_s and Q_w, we varied Q_s and Q_w (and therefore τ) independently and widely. In nature Q_s and Q_w are coupled as sediment flux increases with discharge, although natural rivers show inherent variability in this relation [e.g., *Rickenmann*, 2001; *Barry et al.*, 2004]. Reasons for variability include limited sediment supply, supply and discharge-dependent bed morphologies including surface layer armoring, and episodic sediment production and transport from hillslopes into channels, leading to large short-term variations in Q_s/Q_t as were observed by *Turowski and Rickenmann* [2008].

[64] The coupling between Q_s and Q_w in natural channels likely is a dominant control on the overall effective relation between shear stress and erosion rate. Our observation that erosion rate was independent of shear stress (Figures 8 and 11) is important for mechanistically understanding the controls on bedrock erosion rates and how to better predict them. However, this result cannot be applied independently of mechanistic sediment flux–dependent models, as it only held true when both sediment flux and sediment cover remained constant. It is highly implausible that sediment flux would remain constant in a natural channel, particularly with changes in discharge and cover. Furthermore, our results show that both tools and cover effects provide effective although nonunique mechanisms by which erosion rate can be positively correlated with shear stress. Because erosion rate increases approximately linearly with sediment flux (Figure 6), a positive relation between Q_s and Q_w would effectively lead to a positive relation between discharge and erosion rate. Similarly, Figures 8 and 11 show that preferential cover at lower discharges (and more relevantly at higher Q_s/Q_t) caused a positive correlation between shear stress and erosion rate (time steps 30–34). In many natural systems, high discharge events may increase alluvial bed deposition and therefore cover effects, while lower discharge events may preferentially remove alluvial cover and erode bedrock [*Turowski et al.*, 2007a; *Turowski and Rickenmann*, 2008; *Johnson et al.*, 2010]. Overall, we expect that positive correlations between shear stress and erosion rate are common in natural bedrock channels in which the dominant erosion mechanism is impact wear. Nonetheless, the mechanisms by which both sediment supply and discharge combine to modulate incision rates can lead to great variability in the relationship between incision rates and shear stress.

5. Conclusions

[65] Using flume experiments we systematically varied sediment flux and water discharge and to a large extent isolated the competing influences of sediment flux, sediment cover, shear stress and evolving channel morphology on bedrock channel erosion rate. We found that erosion rate is linearly proportional to sediment flux, and is also inhibited by alluvial cover effects, both consistent with the saltation-abrasion model for bedrock channel incision [*Sklar and Dietrich*, 2004]. Thresholds in bed roughness and in the ratio of sediment flux to transport capacity had to be overcome before alluviation would occur. The extent of static alluvial cover increased with the ratio of sediment flux to transport capacity, but also depended on local bed topography. In our experiments, static alluvial cover was effective at inhibiting local erosion. However, we found no evidence of dynamic cover effects, hypothesized by *Turowski et al.* [2007b] to cause a reduction in local bedrock incision under mobile bed load at high sediment concentrations.

[66] When both sediment flux and alluvial cover were held constant over most of the range of shear stress for which sediment travels as bed load (i.e., prior to partial suspension), we found that there was no direct dependence of erosion rate on flume-averaged shear stress (controlled by varying discharge while holding flume slope fixed). This finding is inconsistent with the saltation-abrasion model which predicts a negative dependence of erosion rate on shear stress, all else held equal. However, in natural channels sediment flux will be correlated with discharge and shear stress. The mechanistic relation between shear stress and erosion in natural abrasion-dominated bedrock channels may thus be dominantly controlled by sediment flux and size, discharge, bed cover and channel morphology.

[67] Our results emphasize that bed roughness should be explicitly incorporated into models of bedrock channel incision and models of channel dynamics in general, as roughness affects local shear stress, sediment transport and sediment deposition. Bed topography evolved to form an inner channel, increasing roughness during the experiments. The observed lack of erosional dependence on shear stress may reflect tradeoffs between sediment impact intensities and particle transport paths as they interact with locally rough bed topography. Erosion was focused on upstream-facing surfaces, even when the amplitude of bed roughness was small. We also found that variations in imposed Q_s and Q_w caused variations in sediment cover, which in turn inhibited the growth of local bed roughness along the inner channel because erosion was preferentially focused on topographic highs but inhibited in local lows. Thus we infer that magnitude-frequency variations in discharge and sediment flux may stabilize bed roughness in natural incising channels.

[68] **Acknowledgments.** This work was supported by NSF Hydrological Sciences and Geomorphology and Land Use Dynamics programs through grant EAR-0821613 (originally EAR-0439037) and the National

Center for Earth-Surface Dynamics. We thank Katrina Cornell, Sarah Gelman, Mariela Perignon, James Buttles, David Mohrig, and Brandon McElroy for invaluable assistance in the lab. Comments on an earlier draft by Daniel Malmon and Eric Horsman and reviews by Mikael Attal, two anonymous reviewers, and A.E. Simon Mudd improved the manuscript greatly.

References

Barabasi, A. L., and H. E. Stanley (1995), *Fractal Concepts in Surface Growth*, Cambridge Univ. Press, Cambridge, U. K.

Barry, J. J., J. M. Buffington, and J. G. King (2004), A general power equation for predicting bed load transport rates in gravel bed rivers, *Water Resour. Res.*, *40*, W10401, doi:10.1029/2004WR003190.

Brocard, G. Y., and P. A. van der Beek (2006), Influence of incision rate, rock strength, and bedload supply on bedrock river gradients and valley-flat widths: Field-based evidence and calibrations from western Alpine rivers (southeast France), *Spec. Pap. Geol. Soc. Am.*, *398*, 101–126.

Chatanantavet, P., and G. Parker (2006), Experimental studies on the rate of incision by saltating abrasion: Verification, analysis and revision of a physically based model, *Eos Trans. AGU*, *87*(52), Fall Meet. Suppl., Abstract H21E–1423.

Chatanantavet, P., and G. Parker (2008), Experimental study of bedrock channel alluviation under varied sediment supply and hydraulic conditions, *Water Resour. Res.*, *44*, W12446, doi:10.1029/2007WR006581.

Chatanantavet, P., and G. Parker (2009), Physically based modeling of bedrock incision by abrasion, plucking, and macroabrasion, *J. Geophys. Res.*, *114*, F04018, doi:10.1029/2008JF001044.

Cowie, P. A., A. C. Whittaker, M. Attal, G. Roberts, G. E. Tucker, and A. Ganas (2008), New constraints on sediment-flux-dependent river incision: Implications for extracting tectonic signals from river profiles, *Geology*, *36*, 535–538, doi:10.1130/G24681A.1.

Dancey, C. L., P. Diplas, A. Papanicolaou, and M. Bala (2002), Probability of individual grain movement and threshold condition, *J. Hydraul. Eng.*, *128*(12), 1069–1075, doi:10.1061/(ASCE)0733-9429(2002)128:12(1069).

Davis, J. R., L. S. Sklar, G. I. Demeter, J. P. Johnson, and K. X. Whipple (2005), The influence of bed roughness on partial alluviation in an experimental bedrock channel, *Eos Trans. AGU*, *86*(52), Fall Meeting Suppl., Abstract H53D–0508.

Fernandez Luque, R., and R. van Beek (1976), Erosion and transport of bedload sediment, *J. Hydraul. Res.*, *14*, 127–144.

Finnegan, N. J., L. S. Sklar, and T. K. Fuller (2007), Interplay of sediment supply, river incision, and channel morphology revealed by the transient evolution of an experimental bedrock channel, *J. Geophys. Res.*, *112*, F03S11, doi:10.1029/2006JF000569.

Gasparini, N. M., R. L. Bras, and K. X. Whipple (2006), Numerical modeling of non-steady-state river profile evolution using a sediment-flux-dependent incision model, *Spec. Pap. Geol. Soc. Am.*, *398*, 127–141, doi:10.1130/2006.2398(08).

Hartshorn, K., N. Hovius, W. B. Dade, and R. L. Slingerland (2002), Climate-driven bedrock incision in an active mountain belt, *Science*, *297*(5589), 2036–2038, doi:10.1126/science.1075078.

Howard, A. D., and G. Kerby (1983), Channel changes in Badlands, *Geol. Soc. Am. Bull.*, *94*(6), 739–752, doi:10.1130/0016-7606(1983)94<739:CCIB>2.0.CO;2.

Howard, A. D., W. E. Dietrich, and M. A. Seidl (1994), Modeling fluvial erosion on regional to continental scales, *J. Geophys. Res.*, *99*, 13,971–13,986, doi:10.1029/94JB00744.

Johnson, J. P., and K. X. Whipple (2007), Feedbacks between erosion and sediment transport in experimental bedrock channels, *Earth Surf. Processes Landforms*, *32*, 1048–1062, doi:10.1002/esp.1471.

Johnson, J. P. L., K. X. Whipple, L. S. Sklar, and T. C. Hanks (2009), Transport slopes, sediment cover, and bedrock channel incision in the Henry Mountains, Utah, *J. Geophys. Res.*, *114*, F02014, doi:10.1029/2007JF000862.

Johnson, J. P. L., K. X. Whipple, and L. S. Sklar (2010), Contrasting bedrock incision rates from snowmelt and flash floods in the Henry Mountains, Utah, *Geol. Soc. Am. Bull.*, in press.

Lamb, M. P., W. E. Dietrich, and J. G. Venditti (2008), Is the critical Shields stress for incipient sediment motion dependent on channel-bed slope?, *J. Geophys. Res.*, *113*, F02008, doi:10.1029/2007JF000831.

Nino, Y., F. Lopez, and M. Garcia (2003), Threshold for particle entrainment into suspension, *Sedimentology*, *50*(2), 247–263, doi:10.1046/j.1365-3091.2003.00551.x.

Parker, G. (1991), Selective sorting and abrasion of river gravel. 1: Theory, *J. Hydraul. Eng.*, *117*(2), 131–149, doi:10.1061/(ASCE)0733-9429(1991)117:2(131).

Rickenmann, D. (2001), Comparison of bed load transport in torrents and gravel bed streams, *Water Resour. Res.*, *37*, 3295–3305, doi:10.1029/2001WR000319.

Rouse, H. (1937), Modern conceptions of the mechanics of turbulence, *Trans. Am. Soc. Civ. Eng.*, *90*, 463–543.

Shepherd, R. G., and S. A. Schumm (1974), Experimental study of river incision, *Geol. Soc. Am. Bull.*, *85*, 257–268, doi:10.1130/0016-7606(1974)85<257:ESORI>2.0.CO;2.

Sklar, L., and W. E. Dietrich (1998), River longitudinal profiles and bedrock incision models: Stream power and the influence of sediment supply, in *Rivers Over Rock: Fluvial Processes in Bedrock Channels*, *Geophys. Monogr. Ser.*, vol. 107, edited by K. J. Tinkler and E. E. Wohl, pp. 237–259, AGU, Washington, D. C.

Sklar, L. S., and W. E. Dietrich (2001), Sediment and rock strength controls on river incision into bedrock, *Geology*, *29*, 1087–1090, doi:10.1130/0091-7613(2001)029<1087:SARSCO>2.0.CO;2.

Sklar, L. S., and W. E. Dietrich (2004), A mechanistic model for river incision into bedrock by saltating bed load, *Water Resour. Res.*, *40*, W06301, doi:10.1029/2003WR002496.

Sklar, L. S., and W. E. Dietrich (2006), The role of sediment in controlling steady-state bedrock channel slope: Implications of the saltation-abrasion incision model, *Geomorphology*, *82*(1-2), 58–83, doi:10.1016/j.geomorph.2005.08.019

Stock, J. D., and D. R. Montgomery (1999), Geologic constraints on bedrock river incision using the stream power law, *J. Geophys. Res.*, *104*, 4983–4993.

Tinkler, K. J. and J. Parish (1998), Recent adjustments to the long profile of Cooksville Creek, an urbanized bedrock channel in Ontario, in *Rivers Over Rock: Fluvial Processes in Bedrock Channels*, *Geophys. Monogr. Ser.*, vol. 107, edited by K. J. Tinkler and E. E. Wohl, pp. 167–187, AGU, Washington, D. C.

Turowski, J. M., and D. Rickenmann (2008), Tools and cover effects in bedload transport observation in the Pitzbach, Austria, *Earth Surf. Processes Landforms*, *34*, 26–37, doi:10.1002/esp.1686.

Turowski, J. M., N. Hovius, H. Meng-Long, D. Lague, and C. Men-Chiang (2007a), Distribution of erosion across bedrock channels, *Earth Surf. Processes Landforms*, *33*, 353–363, doi:10.1002/esp.1559.

Turowski, J. M., D. Lague, and N. Hovius (2007b), Cover effect in bedrock abrasion: A new derivation and its implications for the modeling of bedrock channel morphology, *J. Geophys. Res.*, *112*, F04006, doi:10.1029/2006JF000697.

Whipple, K. X., and G. E. Tucker (1999), Dynamics of the stream-power river incision model: Implications for height limits of mountain ranges, landscape response timescales, and research needs, *J. Geophys. Res.*, *104*, 17,661–17,674, doi:10.1029/1999JB900120.

Whipple, K. X., and G. E. Tucker (2002), Implications of sediment-flux-dependent river incision models for landscape evolution, *J. Geophys. Res.*, *107*(B2), 2039, doi:10.1029/2000JB000044.

Whipple, K. X., G. Hancock, and R. Anderson (2000), River incision into Bedrock: Mechanics and relative efficacy of plucking, abrasion, and cavitation, *Geol. Soc. Am. Bull.*, *112*, 490–503, doi:10.1130/0016-7606(2000)112<490:RIIBMA>2.0.CO;2.

Wobus, C. W., B. T. Crosby, and K. X. Whipple (2006a), Hanging valleys in fluvial systems: Controls on occurrence and implications for landscape evolution, *J. Geophys. Res.*, *111*, F02017, doi:10.1029/2005JF000406.

Wobus, C. W., G. E. Tucker, and R. S. Anderson (2006b), Self-formed bedrock channels, *Geophys. Res. Lett.*, *33*, L18408, doi:10.1029/2006GL027182.

Wohl, E. E., and H. Ikeda (1997), Experimental simulation of channel incision into a cohesive substrate at varying gradients, *Geology*, *25*, 295–298.

J. P. L. Johnson, Department of Geological Sciences, University of Texas at Austin, 1 University Station, C9000, Austin, TX 78750, USA.

K. X. Whipple, School of Earth and Space Exploration, Arizona State University, PO Box 871404, Tempe, AZ 85287, USA.